Computer Methods and Programs in Biomedicine Update 8 (2025) 100218

Contents lists available at ScienceDirect

Computer Methods and Programs in Biomedicine Update

journal homepage: www.sciencedirect.com/journal/computer-methods-and-programs-in-biomedicine-update

# An analytical framework for smoking epidemic modeling using fuzzy logic and dual time-delay dynamics

Muhammad Tashfeen [a], Hothefa Shaker Jassim [b], Muhammad Aziz ur Rehman [a], Fazal Dayan [a], Muhammad Adil Sadiq [c,d], Husam A. Neamah [e,f,*]

[a] Department of Mathematics, School of Science, University of Management and Technology, Lahore, Pakistan
[b] Modern College of Business and Science, Muscat, Oman
[c] Department of Mathematics, DCC-KFUPM, Box 5084, Dhahran 31261, Saudi Arabia
[d] Interdisciplinary Research Center for Hydrogen Technologies and Carbon Management, King Fahd University of Petroleum & Minerals, Box 5084, Dhahran 31261, Saudi Arabia
[e] Department of Electrical Engineering and Mechatronics, Faculty of Engineering, University of Debrecen, Ótemető Utca 2-4, 4028 Debrecen, Hungary
[f] Technical Engineering College, Al-Ayen University, Thi-Qar 64001, Iraq

ARTICLE INFO

*Keywords:*
Smoking epidemic model
Fuzzy parameters
Two-delay systems
Sensitivity analysis
Stability analysis
Consistency

ABSTRACT

The process of smoking is divided into several stages and has a clear tendency towards uncertainty and variability, which are not reflected in the traditional models with presumed parameters. To overcome this difficulty, a fuzzy mathematical model is derived to represent smoking dynamics more accurately under uncertainty. The PSRQE model presented and comprises Potential, Social, Regular, Transitional Non-smokers, and Ex-smokers, integrates vital considerations like the chance of developing smoking and the chance of quitting smoking. The model is analyzed by a stability analysis, numerical simulations, and sensitivity analysis of the basic reproduction number $\mathscr{R}_o$. Three algorithms based on the Forward Euler scheme, the Fourth-Order Runge-Kutta (RK-4) treatment method, and the Non-Standard Finite Difference (NSFD) technique are used to obtain numerical solutions. The NSFD scheme is positive and bounded by convergence analysis, and simulation results have shown that it also preserves the structural properties of the model even when the step sizes are larger. Moreover, the influence of time deviations $\tau_1$ and $\tau_2$ on the smoking habits is also examined. It is demonstrated that this framework provides a valuable foundation for comprehending the leading patterns that govern smoking behavior that are required to reduce smoking rates and the related social, health, and economic impacts.

## 1. Introduction

Cigarette smoking has become a worldwide health crisis, and currently, there are >7000 chemical ingredients, which comprise 70 carcinogens that lead to preventable morbidity and mortality. Tobacco smoke contains heavy metals such as cadmium, lead, and arsenic, which increase risks of lung, throat, and bladder cancer [1]. The most addictive substance is nicotine, which distorts the nervous system, wherein the heart rate and blood pressure elevate, and vasoconstriction occurs, creating risks of cardiovascular diseases such as coronary artery disease and stroke. A typical smoker will ingest 1–2 mg of nicotine in each cigarette, building up the health hazards as he smokes day after day. The male smoking rate is high in Southeast Asia (35 %), and a high prevalence is being witnessed in Africa as a result of intensive tobacco marketing. Interventions have resulted in nations with high incomes reducing smoking, but deprived populations still experience less [2]. Carbon monoxide impedes oxygen transportation, deteriorating chronic obstructive lung disease (COPD), and hydrogen cyanide destroys the lobes of the lung called cilia, which prevents the removal of toxins [3]. Tobacco also undergoes pesticides that further predispose lung cancer [4]. Fertility is also altered as smoking adversely affects the sperm quality in men and the ovarian reserve in women, further impacting the population health besides mortality [5]. Tobacco affects 1.36 billion worldwide, of which 80 percent are in low- and middle-income countries (LMICs) where tobacco smoking is common. According to the World Health Organization (WHO), tobacco kills >8 million people every year, of which 7 million result directly from its use and 1.2 million from secondary exposure to tobacco smoke. Tobacco kills TB victims as

* Corresponding author.
*E-mail address:* husam@eng.unideb.hu (H.A. Neamah).

https://doi.org/10.1016/j.cmpbup.2025.100218

Available online 31 August 2025

tobacco smoking may cause 22 percent of death rates among TB patients, and also it reduces life expectancy by 12–13 years [1–5]. The MPOWER framework implemented by WHO in 2008 encourages tobacco use monitoring, protection against passive exposure to cigarettes, the provision of cessation services, risk information warning, prohibition of advertisements, and tax increases [6]. To a 10 percent price change, in LMICs, the consumption drops by between 10 and 45 percent [7]. There are cessation programs such as nicotine replacement therapies and counseling that are effective but less available in LMICs [8]. Smoke-free polices reduce exposure to secondhand smoke by an average of 90 percent in some regions [9,10]. Health risk campaigns, as seen through educational campaigns, amplify the rate of cessation as they are cost-effective [11]. Such methods as Homotopy Perturbation [12] and Reduced Differential Transform [13] contribute to the assessment of interventions and the formation of the public health policy. Models of time delays take into consideration the time-lapse in smoking initiation and cessation, a more realistic touch. Fractional-order models, such as those proposed by Abdullah et al., separate populations into potential, occasional, regular, temporary, and permanent quitters using Caputo Operators to study the stability through Laplace-Adomian Decomposition. This was generalized to a fractional-order model with age dependence, where the Atangana-Baleanu-Caputo derivatives were applied and proved to have existence, uniqueness, and stability [14]. Their fractal-fractional model considers the practices of governmental interventions, and they used Newton polynomials to simulate them [15]. Khan et al. tested fractal-fractional models using Mittag-Leffler kernels that were stable and simulated the transitions of smoking behavior [16].

The origins of mathematical epidemiology date back to 1760 when Daniel Bernoulli analyzed smallpox epidemiology in England [17]. Ross' seminal 1911 study on malaria transmission dynamics significantly advanced the field [18]. Kermack and McKendrick further expanded Ross's work by developing deterministic compartmental models, where the infection rate is expressed with S and I representing susceptible and infected populations, and k as a constant [19–21]. Before this, Enko's 1889 work also contributed to the foundation of deterministic models. Historically, infectious diseases such as influenza, COVID-19, hepatitis, measles, Zika, and malaria have posed severe public health challenges. Mathematical epidemiology has become an indispensable tool in addressing these challenges, enabling precise predictions of epidemic traits and transmission patterns and informing effective control strategies [22–24]. Recent advancements have built upon the Kermack-McKendrick model, with compartmental extensions like Susceptible Infected (SI), Susceptible Infected Recovered (SIR), Susceptible Infected, Exposed and Recovered (SIER), Susceptible Infected, Exposed, Vaccinated, and Recovered (SIEVR), which incorporates reinfection risks [25]. Human memory and awareness also influence disease dynamics. For example, in dengue models such as SIR-SI, heightened awareness reduces interactions between compartments, particularly in endemic settings [26]. Models like Susceptible, Vaccinated, Exposed, Infected, and Recovered (SVEIR) show that vaccinated individuals exhibit greater awareness of past outbreaks, which in turn impacts disease dynamics. Experts must extract relevant data using scientific methods that combine modeling with empirical evidence for informed decision-making. Momani et al. [27] examined the finite-time stability of the fractional-order Chinese pandemics SIR models of COVID-19. They proved the usefulness of the fractional calculus in describing the memory effect and the dynamics of the epidemic in the real world. Fractional-order models were first used to model the effect of memory and heredity in the dynamics of infectious diseases by Ndendya et al. [28]. Renald et al. [29] introduced a new method of studying data error in compartmentalized paradigms, using three unique epidemiological data sets to evaluate uncertainty in transmission dynamics of the Lumpy Skin Disease (LSD) in cattle, using the Adaptive Metropolis Hastings algorithm. The researchers Shewafera et al. [30] modeled Caputo fractional-order pneumonia-based transmission dynamics and stability properties of asymptomatic carriers.

Delayed epidemic models incorporate time delays in disease transmission or response and affect dynamics. Delay mechanisms have been studied by Misra et al. [31], and steady-state solutions and stability have been analyzed, and delay conditions for epidemic prediction have also been found. Time delays can shift the bare heave dynamics, and can lead to oscillations, and/or sudden changes and instability [32–33]. This is peculiar since models with delay differential equations (DDEs) accommodate such factors and conditions as exposure-disease on-ramp, time to vaccinate effectiveness, and recovery time [34–35]. Gosh et al. [36] proposed delays depending on the duration of the disease with distributed, delay, and standard SIR model comparisons. Meziane et al. [37] considered the mathematical model with a two-virus epidemic and delay effects, while Almuqati et al. [38] considered the multi-group epidemic model with logistic growth structure and delay distributions. Fadhal et al. [39] created a four-subpopulation delay differential model of scabies and proved such important properties of the model as positivity, boundedness, and asymptotic stability. The theoretical findings, as well as the numerical experiments, showed that delay-based modeling can contribute to the dynamics and control of an epidemic. Raza et al. [40]. generalized an existing deterministic hepatitis B model into a stochastic delayed model having effects of multicompartments. They investigated relevant properties and stability and demonstrated that a recently proposed stochastic NSFD approach retains all features of dynamics better than established numerical schemes. Minhós et al. [41] formulated a stochastic tank of a fractional delayed heroin model by relying on Delayed Differential Equations (DDEs) to model chance and memory in drug addiction. They defined the main mathematical characteristics and used the Grunwald Letnikov Non-Standard Finite Difference Scheme (GL-NSFD) algorithm to achieve a quick calculation and the simulations' arrival at theory, thus proving the setup information concerning the approach to the depth of control of addictions.

Fuzzy variables emphasize the fact that epidemic models are sensitive to the complexity of the real world and have an element of randomness. Every day in engineering, meteorology, manufacturing, medicine, and decision-making, as previously stated, fuzzy set theory helps to handle uncertainty and variability [42,43]. Fuzzy mathematical models are seen to be very efficient in the modeling of imprecise data inherent in epidemic spread and control parameters. By utilizing fuzzy sets and fuzzy numbers, epidemiological coefficients such as transmission and recovery rates can be described. Uncertainty is the most common type of ambiguity for a simple reason: human language is imprecise, and any expression is rather vague and cannot be defined in black and white. That is why, in analyzing the disease, for example, its intensity within the community, the truth may be completely different, even if it is impossible to achieve the poles and physically stay between the poles, depending on the observer and the conditions. It has been seen that the combination of fuzzy sets, logic, and mathematical modeling has had a significant effect in different branches of academia: antecedent social science components and epidemiology. Fuzzy methods have been explained as effective in the literature reviewed by Abdy et al. [44], Li et al. [45], Shi et al. [46], Stiegelmeier and Bressan [47], and Shaban et al. [48]. These works show how fuzzy models can be applied to disease modeling and decision-making for disease control. For example, Bhuju et al. [49] studied an SIR model of a fuzzy environment, indicating differences in parameters such as vulnerability, infectivity, and recovery rate. Drawing from such essential studies, more advanced fuzzy epidemiological modeling research has been conducted to the present. For instance, Alqarni et al. [50] worked on a fuzzy SEIR Amoebiasis model based on equilibrium analysis and reproductive numbers. What they have done reflects the ability of fuzzy methods to improve the assessment in describing disease processes and designing intervention strategies. Arif et al. [51] concentrate on the current steep rise of disease modeling, which calls for more accurate models by proposing a new computational tool, the Hybrid SIR-Fuzzy Model.

This study has been motivated by the fact that the classical mathematical models are limited by fixed parameters, which do not allow for

uncertainty and variability inherent in real smoking behaviors. The passage of individuals through their potential, social, regular, transitional, non-smoker, and ex-smoker stages is subject to the stochastic influences of individual susceptibility, social pressures, and variability in success rates of cessation that is not well coherent with deterministic models. This uncertainty can be well covered utilizing the fuzzy set theory, thereby providing a more exact determination of the smoking dynamics. The contribution of this study is in the establishment of an innovative fuzzy PSRQE model, which takes into account two time delays to denote possible transitions of behavior, e.g., delays in smoking initiation or smoking quit attempts. Through the application of fuzzy parameters, stability and sensitivity studies, and other highly developed numerical procedures such as the NSFD method, the paper offers a broad basis through which smoking patterns and intervention measures can be understood and applied to a large extent, a breakthrough compared to the current deterministic and fractional-order models. The novelty of the research resides in the development of a fuzzy five-compartment model of smoking dynamics, which incorporates all relevant uncertainties. They are also precisely analyzed in terms of convergence and structural preservation of the NSFD approach with dual delay factors to provide a better understanding of the smoking behavior transitions.

Section 2 introduces a fuzzy delayed epidemic model based on the PSRQE smoking model. Section 3 delves into equilibrium analysis and reproduction number calculations to assess stability, along with its sensitivity. Section 4 outlines numerical methods, comparison of the RK-4, Euler scheme, and the NSFD method and positivity, convergence, and consistency of the NSFD method. Quantitative assessments are provided in this section. Conclusions are based on the results in Section 5.

## 2. Preliminaries

In the following section, we provide some fundamental concepts that will be relevant in this study.

### 2.1. Definition 1

Consider $X$ to be a nonempty classical set. A subset [52] $M$ of $X$ is a fuzzy set, symbolized by $\widetilde{M}$. It is defined as $\widetilde{M} = \{(\sigma, \mu_{\widetilde{M}} : \sigma \in X)\}$, where $\mu_{\widetilde{M}} : X \to [0,1]$ represents the membership function associated with a fuzzy set $\widetilde{M}$, describing the degree to which $\sigma$ sigma belongs to X.

### 2.2. Definition 2

Let $\widetilde{M}$ be a fuzzy set. We denote any element of $\widetilde{M}$ as a fuzzy number [52] if the universal set $X = \mathbb{R}$, and the membership function has the following properties,

- $\exists$ at least one $\sigma \in \mathbb{R}$ such as $\widetilde{F}$ is standardized fuzzy set (*i.e.*, $\mu_M(\sigma) = 1$),
- $\mu_{\widetilde{M}}$ is convex,
- The membership function $\widetilde{M}$ is continuous in a piecewise manner.
- The support of $\mu_{\widetilde{M}}$ is finite, as support $= \{\sigma : \mu_{\widetilde{M}}(\sigma) > 0\} \subset \mathbb{R}$.

### 2.3. Definition 3

A fuzzy number is considered triangular as defined in [52] if its membership function $\mu_{\widetilde{A}}(\sigma)$ is defined as follows:

$$\mu_{\widetilde{A}}(\sigma) = \begin{cases} 0, & \sigma \le l \\ \dfrac{\sigma - l}{m - l}, & l \le \sigma \le m \\ \dfrac{n - \sigma}{n - m}, & m < \sigma \le n. \end{cases} \tag{1}$$

Where $l \le m \le n$.

### 2.4. Definition 4

The anticipated value of a triangular fuzzy number $\widetilde{A}$ is given by [53]

$$E(\widetilde{A}) = \frac{a + 2b + c}{4}. \tag{2}$$

### 2.5. Classical smoking model

We considered the PSRQE smoking model as presented by Pavani et al. [54].

$$\begin{cases} \dfrac{dP}{dt} = \pi - \beta PR - \mu P, \\ \dfrac{dS}{dt} = \beta PR - (\omega_1 + \mu)S, \\ \dfrac{dR}{dt} = \omega_1 S + \omega_2 RQ - (\psi + \mu)R, \\ \dfrac{dQ}{dt} = \psi(1 - \varphi)R - \omega_2 RQ - \mu Q, \\ \dfrac{dE}{dt} = \varphi\psi R - \mu E. \end{cases} \tag{3}$$

### 2.6. Fuzzy-Based smoking model

A scheme is considered where its parameters are better described using fuzzy sets instead of point values. Here, a parameter is characterized by a fuzzy set, and each of the membership functions covers all the possible values. This method enables an efficient way of handling the vagueness, imprecision, or irregularity in the framework. It is beneficial when empirical evidence is shifting or when inherent random errors compromise the system. Indeed, it is necessary to emphasize that fuzzy parameters are more appropriate to be used instead of fixed parameters in probabilistic models, in different conditions and contexts.

The corresponding fuzzy model for the above system is expressed as:

$$\begin{cases} \dfrac{dP}{dt} = \pi - \beta(\sigma)PR - \mu P, \\ \dfrac{dS}{dt} = \beta(\sigma)PR - (\omega_1 + \mu)S, \\ \dfrac{dR}{dt} = \omega_1 S + \omega_2 RQ - (\psi(\sigma) + \mu)R, \\ \dfrac{dQ}{dt} = \psi(\sigma)(1 - \varphi(\sigma))R - \omega_2 RQ - \mu Q, \\ \dfrac{dE}{dt} = \varphi(\sigma)\psi(\sigma)R - \mu E. \end{cases} \tag{4}$$

The model for explaining the dynamics of smoking behavior involves distinct compartments that are represented using differential equations. The probable smokers $(P)$, join the population through birth continuously at rate $\pi$, die due to natural causes at rate $\mu$, and effectively interact with the social smokers $(S)$, at a rate $\beta(\sigma)$ independent of the level of concentration, social smokers transition to regular smoking habits at a rate $\omega_1$, but dies naturally at rate $\mu$. Regular smokers change to a state of interim quitters $(Q)$, at a rate $\psi(\sigma)$, if they cannot quit smoking permanently at a rate $1 - \varphi(\sigma)$; if they succeed in quitting permanently at a rate $\varphi(\sigma)$, they move to ex-smokers $(E)$. Interim quitters of smoke termination are at risk of reverting to regular smoking at a rate $\omega_2$, and are also affected by a natural death at a rate $\mu$. Ex-smokers $(E)$ are a part of the population that has successfully stopped smoking, departing from being regular smokers at $\varphi(\sigma)\psi(\sigma)$ and dying at a rate of $\mu$. The transition rates from one compartment to another, smoking termination rates, and relapse rates are taken as fuzzy parameters to describe variability and randomness in the smoking behavior and effects

of interventions. These parameters are denoted as $\beta(\sigma)$, $\psi(\sigma)$, and $\varphi(\sigma)$, respectively, and are defined as:

$$\beta(\sigma) = \begin{cases} 0, \ \sigma \leq \sigma_{min} \\ \dfrac{\sigma - \sigma_{min}}{\sigma_{max} - \sigma_{min}}, \ \sigma_{min} < \sigma \leq \sigma_{max} \\ 1, \ \sigma_{max} \leq \sigma. \end{cases} \tag{5}$$

Where $\sigma_{min}$ assumes the minimum possible value for the variable $\sigma$, and $\sigma_{max}$ assumes the maximum possible value for the same variable, defining the zone in which the function $\beta(\sigma)$ changes its character and becomes constant.

$$\psi(\sigma) = \begin{cases} \dfrac{(1-\xi) - \alpha_0}{\sigma_{min}}\sigma + \alpha_0, \ 0 \leq \sigma \leq \sigma_{min} \\ 1 - \xi, \ \sigma_{min} < \sigma. \end{cases} \tag{6}$$

Where $\alpha_0$ is a constant coefficient in the function $\psi(\sigma)$, defining the straight line for the value of $\sigma$ within the range of $0 \leq \sigma \leq \sigma_{min}$, $\xi$ is a parameter of the function $\psi(\sigma)$ that takes the fixed value when $\sigma_{min} < \sigma$, and

$$\varphi(\sigma) = \frac{(\varphi_0 - 1)}{\sigma_{max}}\sigma + 1. \ 0 \ \leq \sigma \leq \sigma_{min}. \tag{7}$$

Where $\varphi_0$ is a constant coefficient in $\varphi(\sigma)$ that examines the value of the linear function within the permissible interval of $0 \ \leq \sigma \leq \sigma_{min}$.

### 2.7. Fuzzy delayed smoking model

A significant delay between infection and transmission is accounted for in most differential epidemic models, making delayed epidemic models essential for explaining disease dynamics. In the context of the smoking dynamics model, two significant delays, $\tau_1$ and $\tau_2$, are considered to represent the progression through various smoking-related compartments better. The delay $\tau_1$ corresponds to the time taken for potential smokers to transition into social smokers, while $\tau_2$ reflects the time required for social smokers to become regular smokers or quitters. The factors $e^{-\mu\tau_1}$ and $e^{-\mu\tau_2}$ capture the effects of natural mortality or termination during these respective periods. To enhance the accuracy of the model and reflect these dynamics more comprehensively, the fuzzy delayed smoking model incorporates the terms $(t - \tau_1)$ $e^{-\mu\tau_1}$ and $(t - \tau_2)$ $e^{-\mu\tau_2}$. These additions provide a more detailed depiction of the interactions between the compartments, offering more profound insights into smoking behavior dynamics and the transitions influenced by delays.

The fuzzy PSRQE smoking epidemic model with delays is presented as follows:

$$\begin{cases} \dfrac{dP}{dt} = \pi - \beta(\sigma)P(t-\tau_1) \ R(t-\tau_1)e^{-\mu\tau_1} - \mu P, \\ \dfrac{dS}{dt} = \beta(\sigma)P(t-\tau_1)R(t-\tau_1)e^{-\mu\tau_1} - (\omega_1 + \mu)S, \\ \dfrac{dR}{dt} = \omega_1 S + \omega_2 R(t-\tau_2)Q(t-\tau_2)e^{-\mu\tau_2} - (\psi(\sigma) + \mu)R, \\ \dfrac{dQ}{dt} = \psi(\sigma)(1-\varphi(\sigma))R - \omega_2 R(t-\tau_2)Q(t-\tau_2)e^{-\mu\tau_2} - \mu Q, \\ \dfrac{dE}{dt} = \varphi(\sigma)\psi(\sigma)R - \mu E. \end{cases} \tag{8}$$

### 2.7. The fuzzy basic transmission number BTN ($\mathscr{R}_0^f$)

The basic transmission number $\mathscr{R}_0$ represents the average number of individuals influenced to initiate smoking behaviors by a single smoker within a fully susceptible population. To compute the basic transmission number, we apply the next-generation matrix method. Now, from the system (8), we can obtain the vectors for the new smokers and transition terms, respectively, as

$$f = \begin{bmatrix} \beta(\sigma)PRe^{-\mu\tau_1} \\ 0 \\ 0 \end{bmatrix}, \ v = \begin{bmatrix} (\omega_1 + \mu)S \\ -\omega_1 S - \omega_2 RQe^{-\mu\tau_2} + (\psi(\sigma) + \mu)R \\ -\psi(\sigma)(1-\varphi(\sigma))R + \omega_2 RQe^{-\mu\tau_2} + \mu Q \end{bmatrix}.$$

$\mathscr{F}$ and $\mathscr{V}$ are now the Jacobians of $f$ and $v$, respectively, at the smoke-free equilibrium (SFE).

$$\mathscr{F} = \begin{bmatrix} 0 & \beta(\sigma)Pe^{-\mu\tau_1} & 0 \\ 0 & 0 & 0 \\ 0 & 0 & 0 \end{bmatrix}, \ \mathscr{V} = \begin{bmatrix} (\omega_1 + \mu) & 0 & 0 \\ -\omega_1 & (\psi(\sigma) + \mu) & 0 \\ 0 & -\psi(\sigma)(1-\varphi(\sigma)) & \mu \end{bmatrix}.$$

Now,

$$\mathscr{V}^{-1} = \begin{bmatrix} \dfrac{1}{(\omega_1 + \mu)} & 0 & 0 \\ \dfrac{\omega_1}{\mu^2 + \mu\omega_1 + \mu\psi(\sigma) + \omega_1\psi(\sigma)} & \dfrac{1}{(\psi(\sigma) + \mu)} & 0 \\ \dfrac{-\omega_1\varphi(\sigma)\psi(\sigma) + \omega_1\psi(\sigma)}{\mu^3 + \mu^2\omega_1 + \mu^2\psi(\sigma) + \mu\omega_1\psi(\sigma)} & \dfrac{-\varphi(\sigma)\psi(\sigma) + \psi(\sigma)}{\mu^2 + \mu\psi(\sigma)} & \dfrac{1}{\mu} \end{bmatrix},$$

The basic transmission number, $\mathscr{R}_o$ is the spectral radius of the next-generation matrix, the spectral radius of $\mathscr{F}\mathscr{V}^{-1}$ is

$$\mathscr{R}_o = \frac{\beta(\sigma)\omega_1\pi e^{-\mu\tau_1}}{\mu(\omega_1 + \mu)(\psi(\sigma) + \mu)}.$$

The BTN $\mathscr{R}_o$ by inserting the SFE point is given by

$$\mathscr{R}_0 = \frac{\beta(\sigma)\omega_1\pi e^{-\mu\tau_1}}{\mu k_1 k_2}.$$

Where, $k_1 = (\omega_1 + \mu), k_2 = (\psi(\sigma) + \mu)$.

The FBTN number $\mathscr{R}_0$ can be analyzed as follows:

**Case 1:** If $\sigma \leq \sigma_{min}$, then we have $\beta(\sigma) = 0$, and we obtain

$$\mathscr{R}_0(\sigma) = 0.$$

**Case 2:** If $\sigma_{min} < \sigma \leq \sigma_{max}$, then we have $\beta(\sigma) = \frac{\sigma - \sigma_{min}}{\sigma_{max} - \sigma_{min}}$, and we obtain,

$$\mathscr{R}_0(\sigma) = \frac{\beta(\sigma)\omega_1\pi e^{-\mu\tau_1}}{\mu k_1 k_2}.$$

**Case 3:** If $\sigma_{max} \leq \sigma$, we have $\beta(\sigma) = 1$ and we obtain

$$\mathscr{R}_0(\sigma) = \frac{\omega_1\pi e^{-\mu\tau_1}}{\mu k_1 k_2}.$$

$\mathscr{R}_0(\sigma)$ can be written as

$$\mathscr{R}_0(\sigma) = \left(0, \frac{\beta(\sigma)\omega_1\pi e^{-\mu\tau_1}}{\mu k_1 k_2}, \frac{\omega_1\pi e^{-\mu\tau_1}}{\mu k_1 k_2}\right).$$

The fuzzy transmission number can be written as defined in [53]

$$\mathscr{R}_0^f = E[\mathscr{R}_0(\sigma)],$$

$$\mathscr{R}_0^f = \frac{\omega_1\pi e^{-\mu\tau_1}(2\beta(\sigma) + 1)}{4\mu k_1 k_2}. \tag{9}$$

### 2.8. Sensitivity analysis of $\mathscr{R}_0$

The proposed smoking model, as described in the system (8), is analyzed through sensitivity analysis of transmission number $\mathscr{R}_0$ to evaluate the influence of various parameters on its dynamics. Sensitivity analysis provides a deeper understanding of how individual parameters influence the overall behavior of the system. By systematically adjusting one or more parameters within predefined bounds, the analysis identifies the factors that have the most significant impact on smoking behaviors and transitions. Additionally, it highlights parameters that can be modified with minimal effect on other processes within the model. This knowledge is particularly valuable for identifying optimal

intervention points and developing effective control strategies.

We compute derivatives in order to confirm the sensitivity of $\mathscr{R}_0$ as follow:

$$\frac{\partial \mathscr{R}_o}{\partial \beta(\sigma)} = \frac{\omega_1 \pi e^{-\mu\tau_1}}{\mu(\omega_1+\mu)(\psi(\sigma)+\mu)},$$

$$\frac{\partial \mathscr{R}_o}{\partial \pi} = \frac{\beta(\sigma)\omega_1 e^{-\mu\tau_1}}{\mu(\omega_1+\mu)(\psi(\sigma)+\mu)}.$$

$$\frac{\partial \mathscr{R}_o}{\partial \omega_1} = \frac{\beta(\sigma)\omega_1 \pi e^{-\mu\tau_1}}{(\omega_1+\mu)^2(\psi(\sigma)+\mu)}.$$

$$\frac{\partial \mathscr{R}_o}{\partial \psi(\sigma)} = -\frac{\beta(\sigma)\omega_1 \pi e^{-\mu\tau_1}}{(\omega_1+\mu)(\psi(\sigma)+\mu)^2},$$

$$\frac{\partial \mathscr{R}_o}{\partial \tau_1} = -\frac{\beta(\sigma)\omega_1 \pi e^{-\mu\tau_1}}{(\omega_1+\mu)(\psi(\sigma)+\mu)},$$

$$\frac{\partial \mathscr{R}_o}{\partial \mu} = -\frac{\beta(\sigma)\omega_1 \pi e^{-\mu\tau_1}\mu(\omega_1+\mu)(\psi(\sigma)+\mu) - \beta(\sigma)\omega_1 \pi e^{-\mu\tau_1}((\omega_1+\mu)(\psi(\sigma)+\mu)+\mu(\psi(\sigma)+\omega_1+2\mu))}{\mu^2(\omega_1+\mu)^2(\psi(\sigma)+\mu)^2}.$$

### 2.9. Sensitivity indices of $\mathscr{R}_0$

The smoking model's sensitivity index evaluates individual parameters' contribution to the system's overall behavior, demonstrating how changes in specific parameters influence the model's outcomes. This analysis enhances researchers' understanding of key parameters that significantly affect smoking initiation, transition, cessation, or relapse behaviors, enabling the implementation of targeted interventions. Additionally, it aids in refining the model for greater accuracy and developing effective strategies to monitor and influence smoking patterns within a population. The sensitivity index of a parameter is defined as follows [55]:

$$\zeta(\upsilon) = \frac{\upsilon}{\mathscr{R}_o} \times \frac{\partial \mathscr{R}_o}{\partial \upsilon}.$$

Where $\zeta$ denotes the sensitivity of the parameter $\nu$. The sensitivity index of $\beta(\sigma)$ is calculated as

$$\zeta(\beta(\sigma)) = \frac{\beta(\sigma)}{\mathscr{R}_o} \times \frac{\partial \mathscr{R}_o}{\partial \beta(\sigma)} = 1.$$

Similarly,

$$\zeta(\pi) = \frac{\pi}{\mathscr{R}_o} \times \frac{\partial \mathscr{R}_o}{\partial \pi} = 1,$$

$$\zeta(\omega_1) = \frac{\omega_1}{\mathscr{R}_o} \times \frac{\partial \mathscr{R}_o}{\partial \omega_1} = \frac{\omega_1}{k_1},$$

$$\zeta(\psi(\sigma)) = \frac{\psi(\sigma)}{\mathscr{R}_o} \times \frac{\partial \mathscr{R}_o}{\partial \psi(\sigma)} = -\frac{\psi(\sigma)}{k_2},$$

$$\zeta(\tau_1) = \frac{\tau_1}{\mathscr{R}_o} \times \frac{\partial \mathscr{R}_o}{\partial \tau_1} = -\tau_1,$$

$$\zeta(\mu) = \frac{\mu}{\mathscr{R}_o} \times \frac{\partial \mathscr{R}_o}{\partial \mu} = -\frac{\mu\tau_1 k_1 k_2 + \mu k_1 + \mu k_2 + k_1 k_2}{k_1 k_2}.$$

Fig. 1 collectively highlights the interconnected dynamics of key parameters influencing smoking ratios, including the basic transmission number $\mathscr{R}_o$, behavioral factors, and intervention measures. Subfigures (a) and (b) emphasize the significance of intervention thresholds and recovery-related parameters. In Figure (a), $\mathscr{R}_o$ decreases as $\tau_1$ or $\omega_1$ increases, with $\omega_1$ having a notably more substantial effect. Figure (b) delves deeper into the relationship between $\psi(\sigma)$ (associated with termination or recovery) and $\omega_1$, showing that $\mathscr{R}_o$ remains low at smaller values of $\psi(\sigma)$but rises significantly at higher values, particularly with increased $\omega_1$, indicating diminished intervention effectiveness due to saturation effects. Figures *c* through *f* explore how demographic, transmission, and control-related factors shape $\mathscr{R}_o$. Figure *c* reveals that $\mathscr{R}_o$ increases with $\beta(\sigma)$ (linked to transmission processes and their uncertainty) but decreases with larger $\tau_1$, showcasing the effectiveness of delayed interventions. Figure *d* highlights the system's sensitivity to specific values of $\mu$ (a demographic parameter) and $\psi(\sigma)$, demonstrating that targeted recovery or cessation strategies can significantly reduce $\mathscr{R}_o$ at higher values, stabilizing the system. Figure *e* examines $\beta(\sigma)$ (related to initiation or relapse rates) and $\pi$ (control measures), showing that $\mathscr{R}_o$ rises with these parameters due to intensified smoking dynamics but declines at their extreme values, reflecting the flattening of intervention impacts. Lastly, Figure F indicates that while $\mathscr{R}_o$ increases with $\beta(\sigma)$, this rise is mitigated by $\omega_1$, underscoring the importance of robust cessation programs.

Together, these figures underscore critical intervention points and thresholds for maximizing impact. They also highlight the interactive nature of behavioral and control parameters, emphasizing the need for adaptive, responsive strategies to address and reduce smoking prevalence within a population effectively.

The bar charts in Fig. 2 illustrate the sensitivity of $\mathscr{R}_o$to various parameters, highlighting the extent to which each influences the basic reproduction number. Among these, $\beta(\sigma)$ displays the highest positive sensitivity index, approximately 0.5, underscoring its critical role in determining $\mathscr{R}_o$ and its strong connection to smoking dynamics and transmission. Similarly, $\pi$ has a positive sensitivity index, though its impact is less pronounced compared to $\beta(\sigma)$, while $\omega_1$ contributes positively with a relatively minor effect. Conversely, $\tau_1$ and $\psi(\sigma)$ exhibit negative sensitivity indices, indicating their effectiveness in reducing $\mathscr{R}_o$. Among these, $\tau_1$ exerts a slightly more substantial negative influence. Notably, $\mu$ stands out as the parameter with the most significant negative sensitivity index, around $-0.4$, demonstrating its pivotal role in substantially lowering $\mathscr{R}_o$ through mechanisms such as increased recovery or cessation rates. This analysis identifies $\beta(\sigma)$ as the most influential parameter for increasing $\mathscr{R}_o$, while $\mu$ is the most impactful in reducing it. Moderate parameters or tiny effects, such as $\omega_1$ (transition rate between social and regular smokers), are kept to retain ecological validity, as their effects can be immense when subjected to changing circumstances or contact with other variables. Eliminating those parameters would oversimplify the model, which decreases the predictive power of the model and its applicability to varied groups. Instead, sensitivity results are used to rank interventions without removing them.

### 2.10. Equilibrium analysis

**Case 1:** If $\sigma \le \sigma_{min}$, then we have $\beta(\sigma) = 0$ and we obtain

$$E_p^0(P^0, S^0, R^0, Q^0, E^0) = (\frac{\pi}{\mu}, 0, 0, 0, 0, 0$$

**Case 2:** If $\sigma_{min} < \sigma \le \sigma_{max}$, then we have $\beta(\sigma) = \frac{\sigma-\sigma_{min}}{\sigma_{max}-\sigma_{min}}$, and we obtain

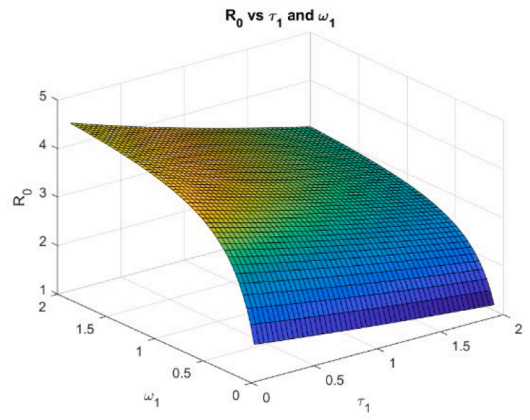


$(a)\ \mathcal{R}_o vs\ \tau_1 and\ \omega_1$

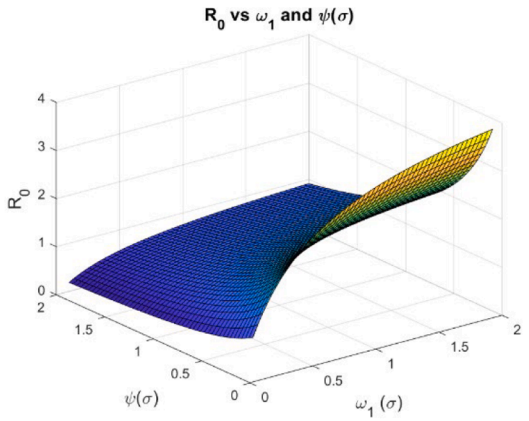


$(b)\ \mathcal{R}_o vs\ \omega_1\ and\ \psi(\sigma)$

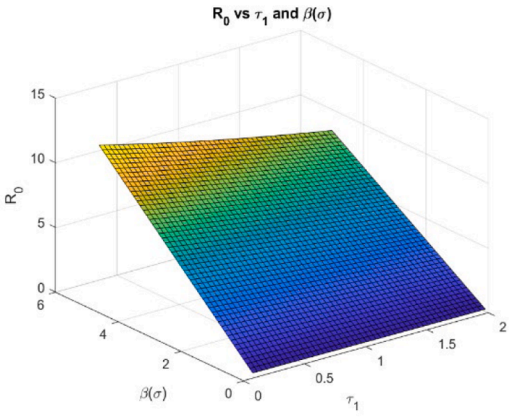


$(c)\ \mathcal{R}_o vs\ \tau_1 and\ \beta(\sigma)$

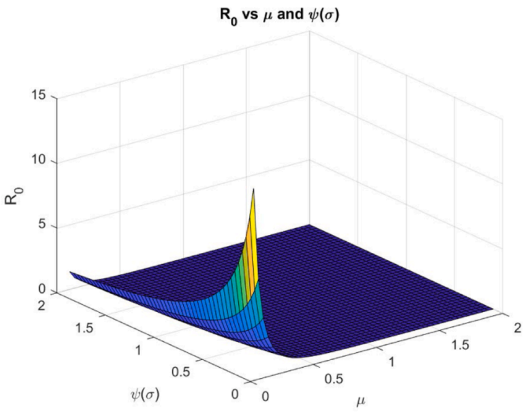


$(d)\ \mathcal{R}_o vs\ \mu\ and\ \psi(\sigma)$

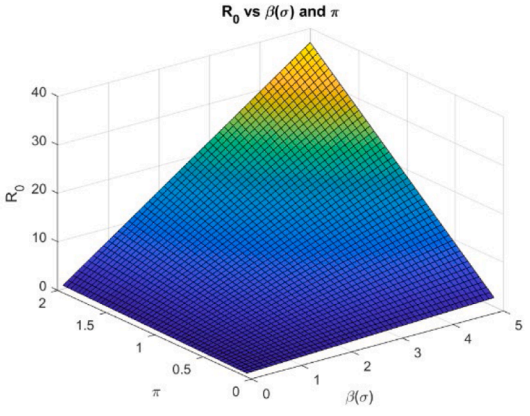


$(e)\ \mathcal{R}_o vs\ \beta(\sigma)\ and\ \pi$

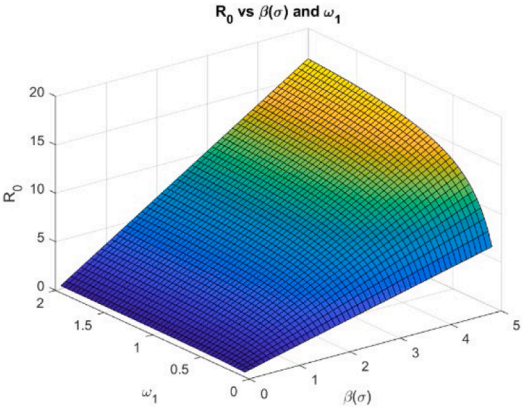


$(f)\ \mathcal{R}_o vs\ \beta(\sigma)\ and\ \omega_1$

**Fig. 1.** Transmission number behavior for the developed system under different parameter effects.

$$P^* = \frac{\pi}{(\beta(\sigma)R^* e^{-\mu\tau_1} + \mu)},$$

$$S^* = \frac{\beta(\sigma)\pi R^* e^{-\mu\tau_1}}{k_1(\beta(\sigma)R^* e^{-\mu\tau_1} + \mu)},$$

$$R^* = \frac{\mu Q^*}{\psi(\sigma)(1-\varphi(\sigma)) - \omega_2 Q^* e^{-\mu\tau_2}},$$

$$Q^* = \frac{\psi(\sigma)(1-\varphi(\sigma))R^*}{\omega_2 R^* e^{-\mu\tau_2} + \mu},$$

$$E^* = \frac{\varphi(\sigma)\psi(\sigma)R^*}{\mu}.$$

**Case 3:** If $\sigma_{max} \leq \sigma$, then we have $\beta(\sigma) = 1$ and we obtain,

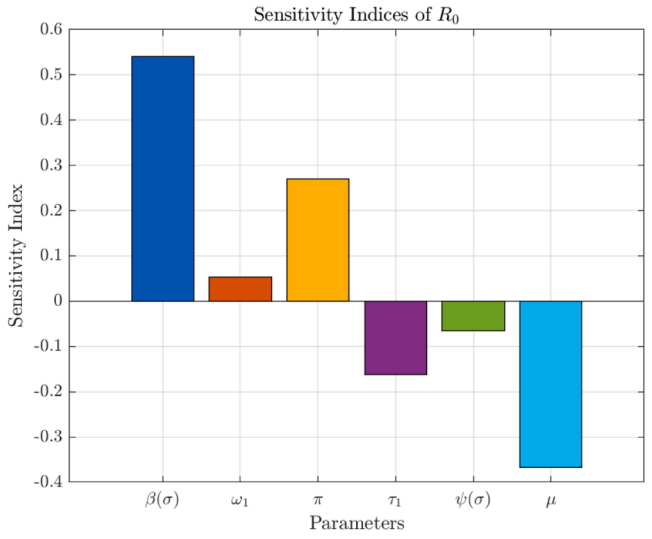


**Fig. 2.** Sensitivity of the basic transmission number $\mathscr{R}_o$.

**Table 1**
Values of parameters.

| Parameters | Values | Parameters | Values | Parameters | Values |
|---|---|---|---|---|---|
| $\pi$ | 3 | $\tau_1$ | $\geq 0$ | $\beta(\sigma)$ | Fuzzy Variable |
| $\mu$ | 0.5 | $\tau_2$ | $\geq 0$ | $\varphi(\sigma)$ | Fuzzy Variable |
| $\omega_1$ | 0.6 | $\omega_1$ | 0.7 | $\psi(\sigma)$ | Fuzzy Variable |

$$P^{**} = \frac{\pi}{(R^{**}e^{-\mu\tau_1} + \mu)},$$

$$S^{**} = \frac{\pi R^{*} e^{-\mu\tau_1}}{k_1(R^{**}e^{-\mu\tau_1} + \mu)},$$

$$R^{**} = \frac{\mu Q^{**}}{\psi(\sigma)(1-\varphi(\sigma)) - \omega_2 Q^{**}e^{-\mu\tau_2}},$$

$$Q^{**} = \frac{\psi(\sigma)(1-\varphi(\sigma))R^{**}}{\omega_2 R^{**}e^{-\mu\tau_2} + \mu},$$

$$E^{**} = \frac{\varphi(\sigma)\psi(\sigma)R^{**}}{\mu}.$$

### 2.11. Stability analysis

The Jacobian matrix of system (8) at the SFE is expressed as follows:

$$J\left(\mathrm{E}_{\mathrm{p}}^{0}\right) = \begin{bmatrix} -\mu & 0 & 0 & 0 & 0 \\ 0 & -k_1 & 0 & 0 & 0 \\ 0 & \omega_1 & -k_2 & 0 & 0 \\ 0 & 0 & \psi(\sigma)(1-\varphi(\sigma)) & -\mu & 0 \\ 0 & 0 & \varphi(\sigma)\psi(\sigma) & 0 & -\mu \end{bmatrix},$$

The above matrix gives us the eigenvalues; $\lambda_1 = -\mu < 0, \lambda_2 = -k_1 < 0, \lambda_3 = -k_2 < 0, \lambda_4 = -\mu < 0, \lambda_5 = -\mu < 0$. By observing that all the eigenvalues of the Jacobian matrix are negative, it can be assumed that the system of differential equations for the PSRQE model exhibits local asymptotic stability at $\mathrm{E}_{\mathrm{p}}^{0}$.

## 3. Numerical modelling

Computational modeling combines mathematical equations with computational tools to construct and analyze complex systems, offering insights and predictions that are often unattainable through direct observation. Several numerical methods and approaches, including the use of finite difference or finite element methods, are used. In this study, the forward Euler scheme, the RK-4 method, and the NSFD method will be applied to analyze the given model.

### 3.1. Forward Euler scheme

The forward Euler method, a widely recognized explicit first-order numerical technique, is commonly used to solve ordinary differential equations. Renowned for its computational efficiency, it provides accurate approximations of solution trajectories over time. In this study, the forward Euler scheme is applied to the aforementioned system (8) as follows;

$$\begin{cases} P^{n+1} = P^n + h(\pi - \beta(\sigma)R^nP^ne^{-\mu\tau_1} - \mu P^n), \\ S^{n+1} = S^n + h(\beta(\sigma)P^nR^ne^{-\mu\tau_1} - k_1S^n), \\ R^{n+1} = R^n + h(\omega_1S^n + \omega_2P^nQ^ne^{-\mu\tau_2} - k_2R^n), \\ Q^{n+1} = Q^n + h(\psi(\sigma)(1-\varphi(\sigma))R^n - \omega_2R^nQ^ne^{-\mu\tau_2} + \mu Q^n), \\ E^{n+1} = E^n + h(\varphi(\sigma)\psi(\sigma)R^n - \mu E^n). \end{cases} \tag{10}$$

### 3.2. Fourth order Runge Kutta scheme (RK-4)

Considering the equations of system (8), an explicit RK-4 method is developed as follows:

Step 1

$$\begin{cases} k_1^P = h[(\pi - \beta(\sigma)P^nR^ne^{-\mu\tau_1} - \mu P^n)], \\ k_1^S = h[\beta(\sigma)P^nR^ne^{-\mu\tau_1} - k_1S^n], \\ k_1^R = h[\omega_1S^n + \omega_2P^nQ^ne^{-\mu\tau_2} - k_2R^n], \\ k_1^Q = h[\psi(\sigma)(1-\varphi(\sigma))R^n - \omega_2R^nQ^ne^{-\mu\tau_2} + \mu Q^n], \\ k_1^E = h[\varphi(\sigma)\psi(\sigma)R^n - \mu E^n]. \end{cases} \tag{11}$$

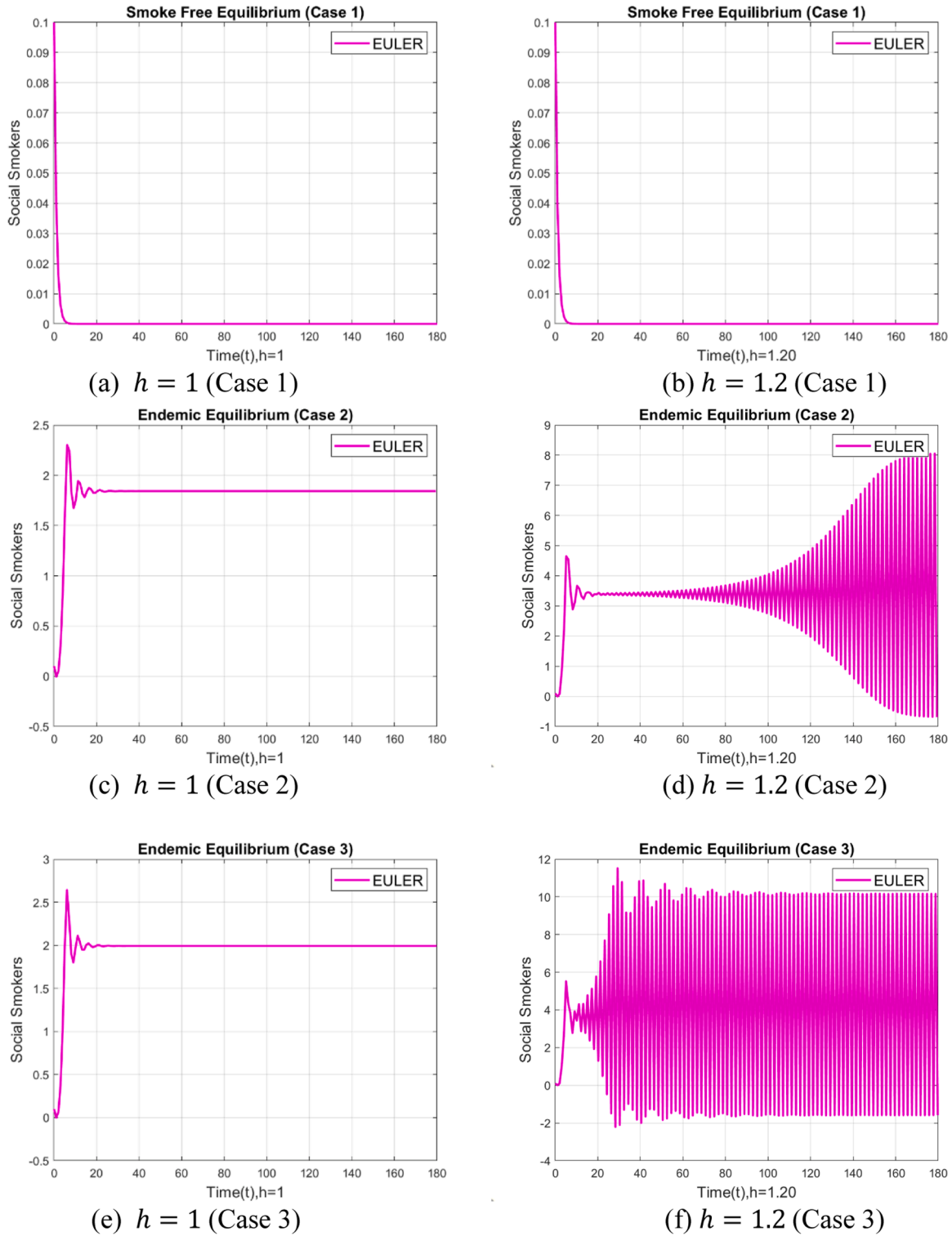


**Fig. 3.** Social smokers at different step intervals utilizing the forward Euler method.

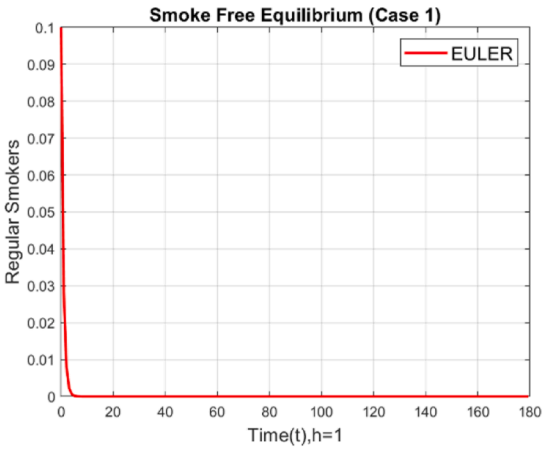


(a) $h = 1$ (Case 1)

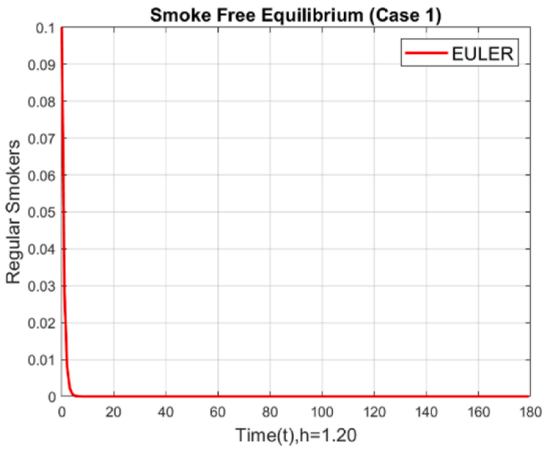


(b) $h = 1.2$ (Case 1)

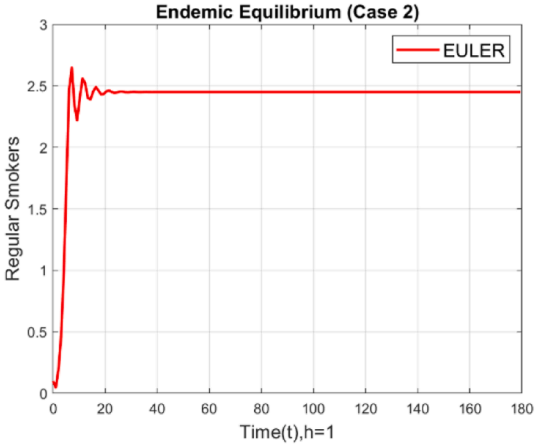


(c) $h = 1$ (Case 2)

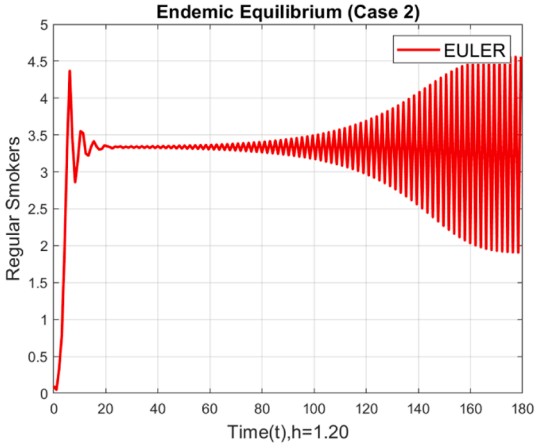


(d) $h = 1.2$ (Case 2)

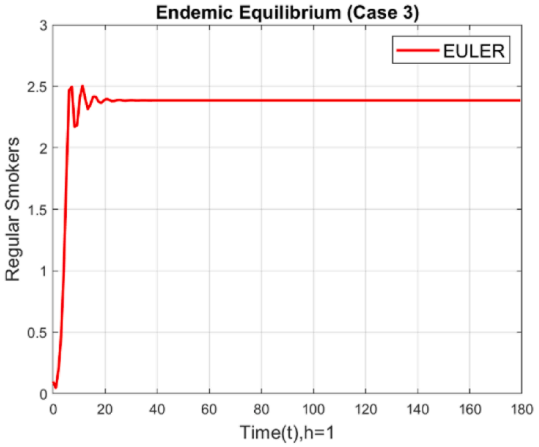


(e) $h = 1$ (Case 3)

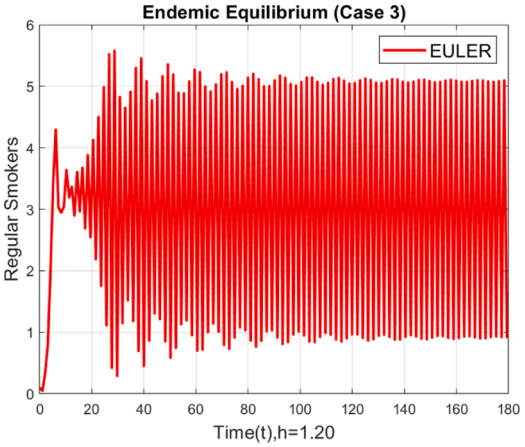


(f) $h = 1.2$ (Case 3)

**Fig. 4.** Regular smokers at different step intervals utilizing the forward Euler method.

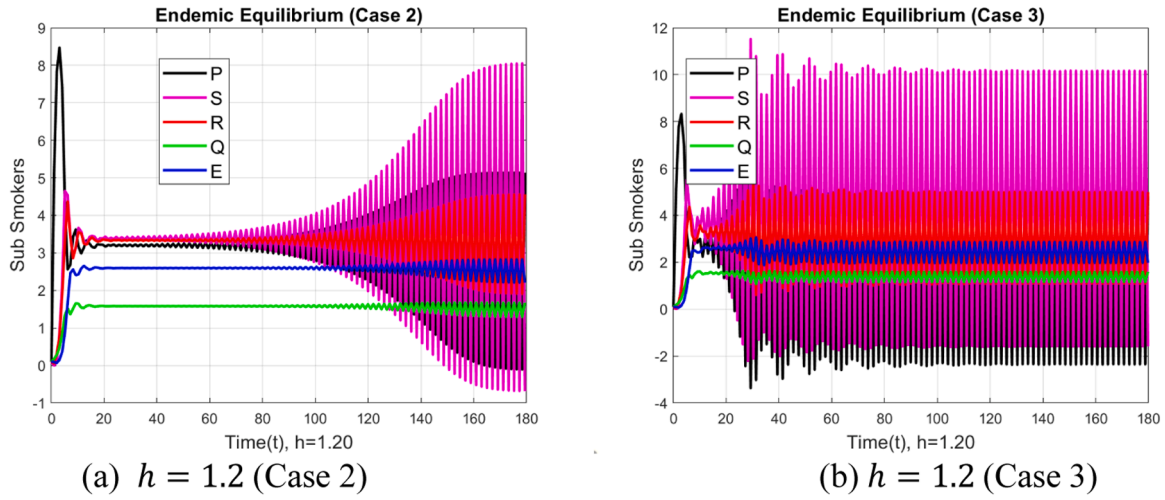


(a) $h = 1.2$ (Case 2) (b) $h = 1.2$ (Case 3)

**Fig. 5.** Compartmental comparison of the PSRQE model utilizing the Forward Euler method.

Step 2

$$\begin{cases} k_2^P = h\left[\left(\pi - \beta(\sigma)\left(P^n + \frac{k_1^P}{2}\right)\left(R^n + \frac{k_1^R}{2}\right)\right)e^{-\mu\tau_1} - \mu\left(P^n + \frac{k_1^P}{2}\right)\right], \\ k_2^S = h\left[\left(\beta(\sigma)\left(P^n + \frac{k_1^P}{2}\right)\left(R^n + \frac{k_1^R}{2}\right)\right)e^{-\mu\tau_1} - k_1\left(S^n + \frac{k_1^S}{2}\right)\right], \\ k_2^R = h\left[\omega_1\left(S^n + \frac{k_1^S}{2}\right) + \omega_2\left(\left(P^n + \frac{k_1^P}{2}\right)\left(Q^n + \frac{k_1^Q}{2}\right)\right)e^{-\mu\tau_2} - k_2\left(R^n + \frac{k_1^R}{2}\right)\right], \\ k_2^Q = h\left[\psi(\sigma)(1-\varphi(\sigma))\left(R^n + \frac{k_1^R}{2}\right) - \omega_2\left(\left(R^n + \frac{k_1^R}{2}\right)\left(Q^n + \frac{k_1^Q}{2}\right)\right)e^{-\mu\tau_2} + \mu\left(Q^n + \frac{k_1^Q}{2}\right)\right], \\ k_2^E = h\left[\varphi(\sigma)\psi(\sigma)\left(R^n + \frac{k_1^R}{2}\right) - \mu\left(E^n + \frac{k_1^E}{2}\right)\right]. \end{cases} \tag{12}$$

***Step 3***

$$\begin{cases} k_3^P = h\left[\left(\pi - \beta(\sigma)\left(P^n + \frac{k_2^P}{2}\right)\left(R^n + \frac{k_2^R}{2}\right)\right)e^{-\mu\tau_1} - \mu\left(P^n + \frac{k_2^P}{2}\right)\right], \\ k_3^S = h\left[\left(\beta(\sigma)\left(P^n + \frac{k_2^P}{2}\right)\left(R^n + \frac{k_2^R}{2}\right)\right)e^{-\mu\tau_1} - k_1\left(S^n + \frac{k_2^S}{2}\right)\right], \\ k_3^R = h\left[\omega_1\left(S^n + \frac{k_2^S}{2}\right) + \omega_2\left(\left(P^n + \frac{k_2^P}{2}\right)\left(Q^n + \frac{k_2^Q}{2}\right)\right)e^{-\mu\tau_2} - k_2\left(R^n + \frac{k_2^R}{2}\right)\right], \\ k_3^Q = h\left[\psi(\sigma)(1-\varphi(\sigma))\left(R^n + \frac{k_2^R}{2}\right) - \omega_2\left(\left(R^n + \frac{k_2^R}{2}\right)\left(Q^n + \frac{k_2^Q}{2}\right)\right)e^{-\mu\tau_2} + \mu\left(Q^n + \frac{k_2^Q}{2}\right)\right], \\ k_3^E = h\left[\varphi(\sigma)\psi(\sigma)\left(R^n + \frac{k_2^R}{2}\right) - \mu\left(E^n + \frac{k_2^E}{2}\right)\right]. \end{cases} \tag{13}$$

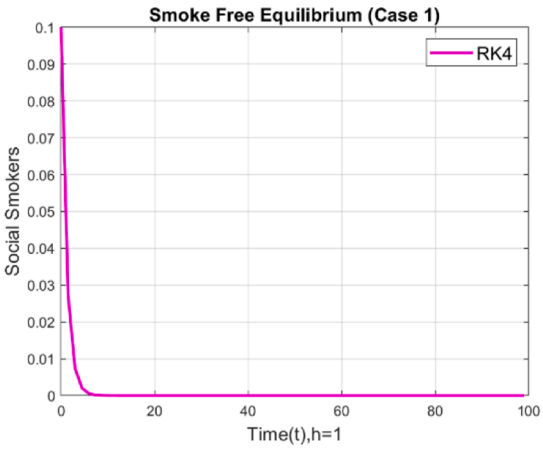


(a) $h = 1$ (Case 1)

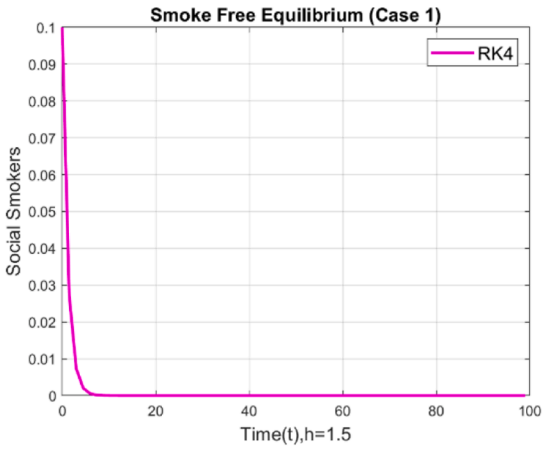


(b) $h = 1.5$ (Case 1)

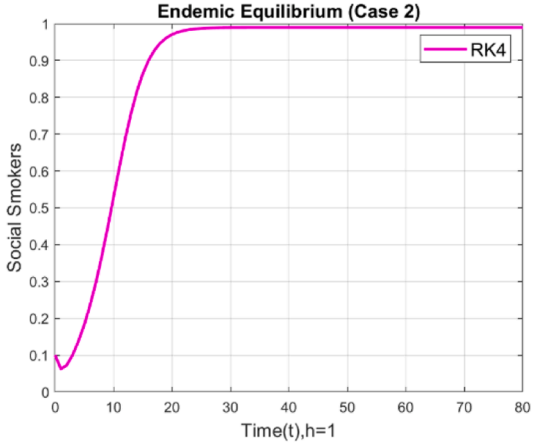


(c) $h = 1$ (Case 2)

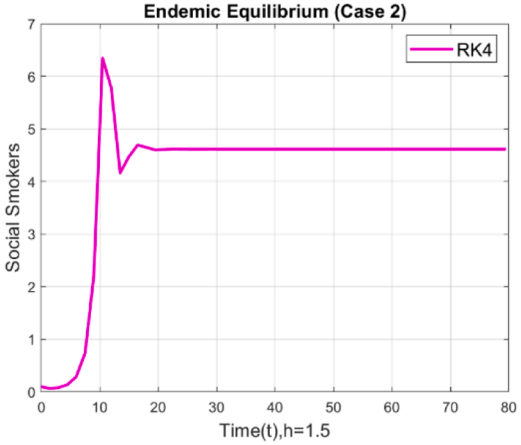


(d) $h = 1.5$ (Case 2)

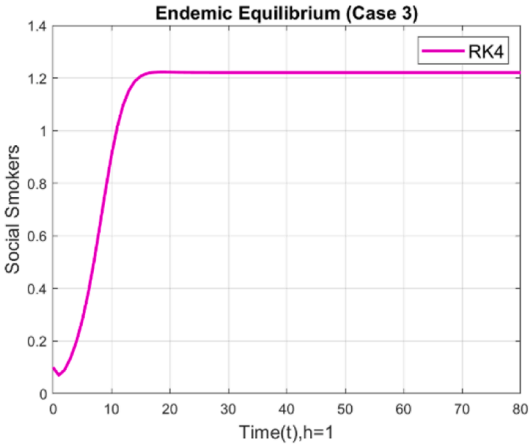


(e) $h = 1$ (Case 3)

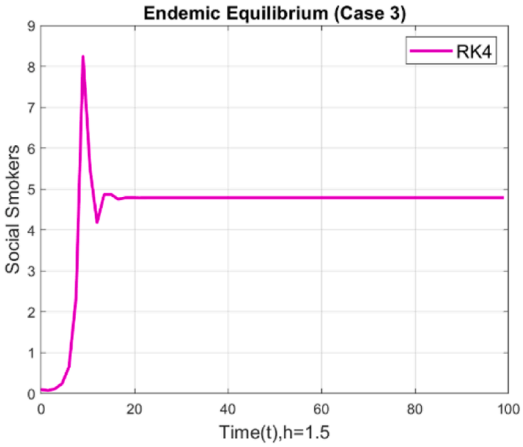


(f) $h = 1.5$ (Case 3)

**Fig. 6.** Social smokers at different step intervals utilizing RK-4 method.

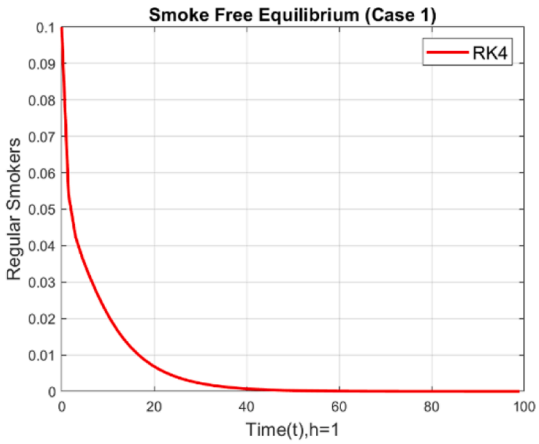


(a) $h = 1$ (Case 1)

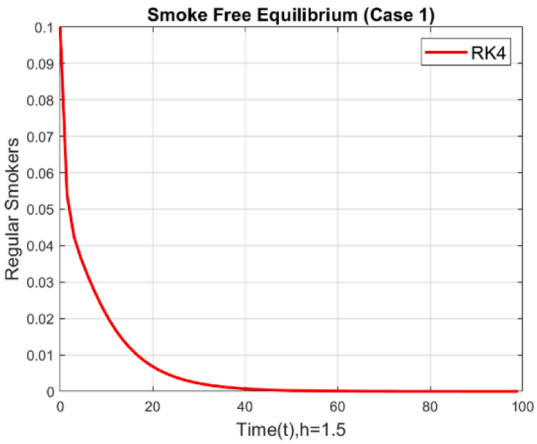


(b) $h = 1.5$ (Case 1)

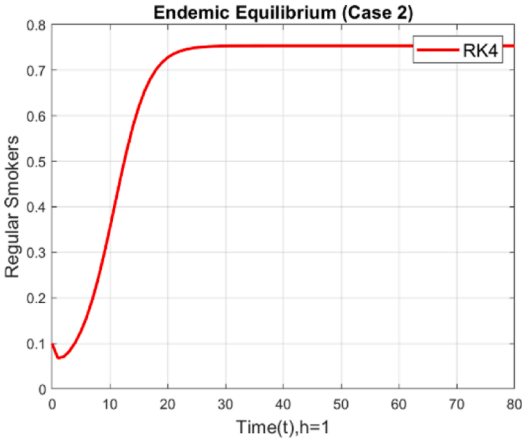


(c) $h = 1$ (Case 2)

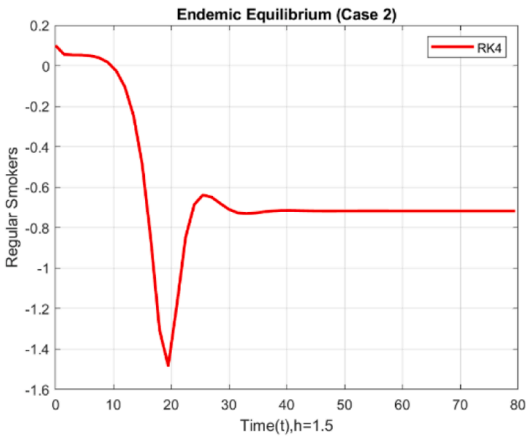


(d) $h = 1.5$ (Case 2)

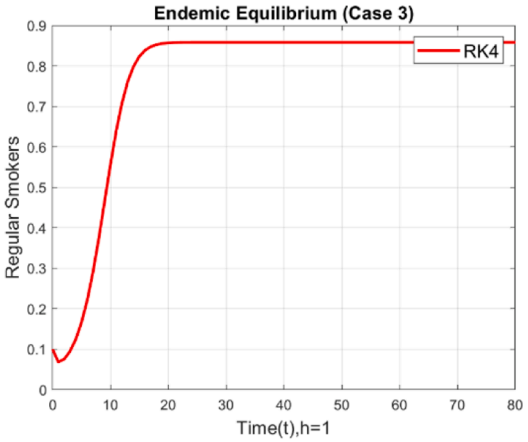


(e) $h = 1$ (Case 3)

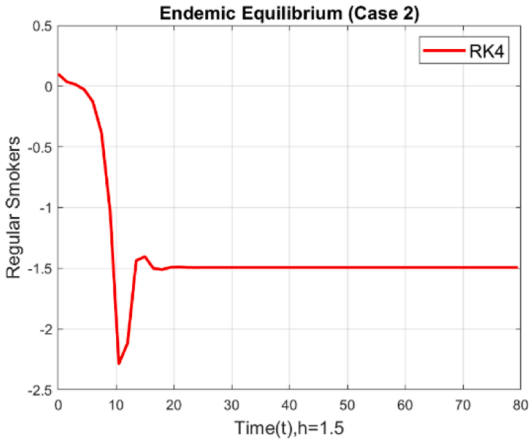


(f) $h = 1.5$ (Case 3)

**Fig. 7.** Regular smokers at different step intervals utilizing RK-4 method.

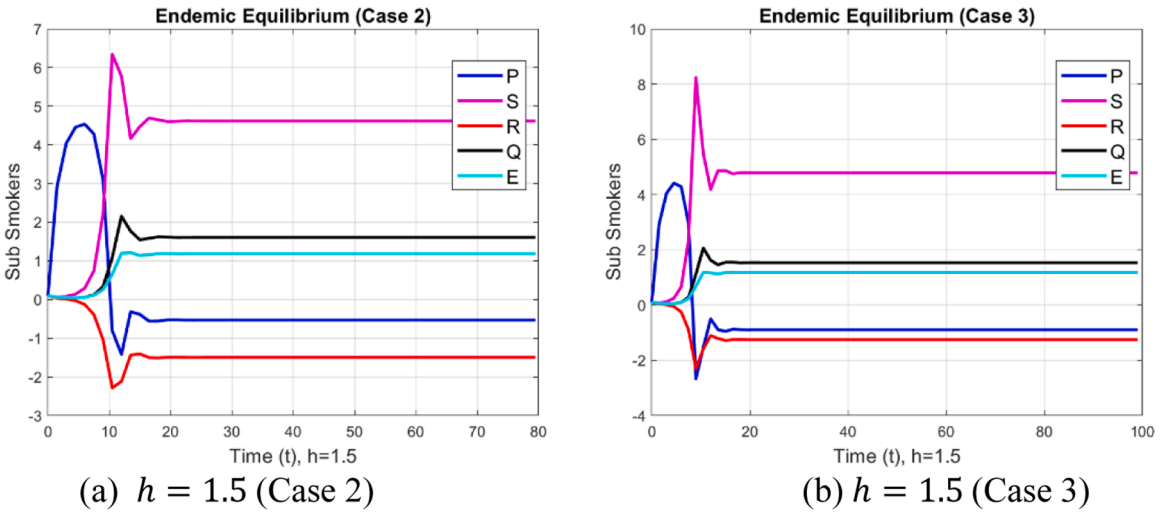


(a) $h = 1.5$ (Case 2) (b) $h = 1.5$ (Case 3)

**Fig. 8.** Compartmental comparison of the PSRQE model utilizing RK-4 method.

***Step 4***

$$\begin{cases} k_4^P = h\left[(\pi - \beta(\sigma)(P^n + k_3^P)(R^n + k_3^R))e^{-\mu\tau_1} - \mu(P^n + k_3^P)\right], \\ k_4^S = h\left[(\beta(\sigma)(P^n + k_3^P)(R^n + k_3^R))e^{-\mu\tau_1} - k_1(S^n + k_3^S)\right], \\ k_4^R = h\left[\omega_1(S^n + k_3^S) + \omega_2((P^n + k_3^P)(Q^n + k_3^Q))e^{-\mu\tau_2} - k_2(R^n + k_3^R)\right], \\ k_4^Q = h\left[\psi(\sigma)(1-\varphi(\sigma))(R^n + k_3^R) - \omega_2((R^n + k_3^R)(Q^n + k_3^Q))e^{-\mu\tau_2} + \mu(Q^n + k_3^Q)\right] \\ k_4^E = h\left[\varphi(\sigma)\psi(\sigma)(R^n + k_3^R) - \mu(E^n + k_3^E)\right]. \end{cases} \tag{14}$$

***Final Step***

$$\begin{cases} P^{n+1} = P^n + \frac{1}{6}\left[k_1^P + 2k_2^P + 2k_3^P + k_4^P\right], \\ S^{n+1} = S^n + \frac{1}{6}\left[k_1^S + 2k_2^S + 2k_3^S + k_4^S\right] \\ R^{n+1} = R^n + \frac{1}{6}\left[k_1^R + 2k_2^R + 2k_3^R + k_4^R\right], \\ Q^{n+1} = Q^n + \frac{1}{6}\left[k_1^Q + 2k_2^Q + 2k_3^Q + k_4^Q\right]), \\ E^{n+1} = E^n + \frac{1}{6}\left[k_1^E + 2k_2^E + 2k_3^E + k_4^E\right]. \end{cases} \tag{15}$$

### 3.3. NSFD scheme

The NSFD method is a sophisticated and efficient approach for solving epidemic models involving fuzzy delayed differential equations. It is recognized as a computational methodology that preserves the essential properties of the continuous model. Key features such as convergence, positivity, and stability are maintained, making the NSFD method particularly well-suited for studying epidemic models. Compared to standard techniques like the Forward Euler Scheme, NSFD methods demonstrate superior computational efficiency and greater alignment with the dynamics of continuous models. In this study, a framework is presented that employs the NSFD approach, incorporating delay factors to enhance its applicability.

$$\begin{cases} P^{n+1} = \dfrac{P^n + h\pi}{1 + h(\beta(\sigma)R^n e^{-\mu\tau_1} + \mu)}, \\ S^{n+1} = \dfrac{S^n + h\beta(\sigma)P^n R^n e^{-\mu\tau_1}}{1 + hk_1}, \\ R^{n+1} = \dfrac{R^n + h(\omega_1 S^n + \omega_2 P^n Q^n e^{-\mu\tau_2})}{1 + hk_2}, \\ Q^{n+1} = \dfrac{Q^n + h(\psi(\sigma)(1-\varphi(\sigma))R^n)}{1 + h(\omega_2 R^n e^{-\mu\tau_2} + \mu)}, \\ E^{n+1} = \dfrac{E^n + h\varphi(\sigma)\psi(\sigma)R^n}{1 + h\mu}. \end{cases} \tag{16}$$

### 3.4. Positivity of the NSFD scheme

Maintaining positivity in the numerical solutions of epidemic models is essential to ensure their applicability and validity. In compartmental epidemic models, at least one state variable representing population segments must remain positive, while all others should be nonnegative. Preserving the positivity of these variables is a critical requirement. This fundamental property is rigorously upheld through the application of mathematical induction within an implicit numerical integration scheme. The following theorem provides valuable insights into this principle.

***Theorem:*** *Let* $P,\ S,\ R,\ Q$ *and* $E \geq 0$ *are finite,* $\geq 0,\ \varphi(\sigma) \geq 0,\ \psi(\sigma) \geq 0, \mu \geq 0, \omega_1 \geq 0, \omega_2 \geq 0, \geq 0, \tau_1 \geq 0, \tau_2 \geq 0$ *and* $\beta(\sigma) \geq 0$, *then* $P^{n+1} \geq 0,\ S^{n+1} \geq 0,\ R^{n+1} \geq 0,\ Q^{n+1} \geq 0,$ *and* $E^{n+1} \geq 0$ *for all* $n \in Z^+$.

The proof is provided in Appendix A.1.

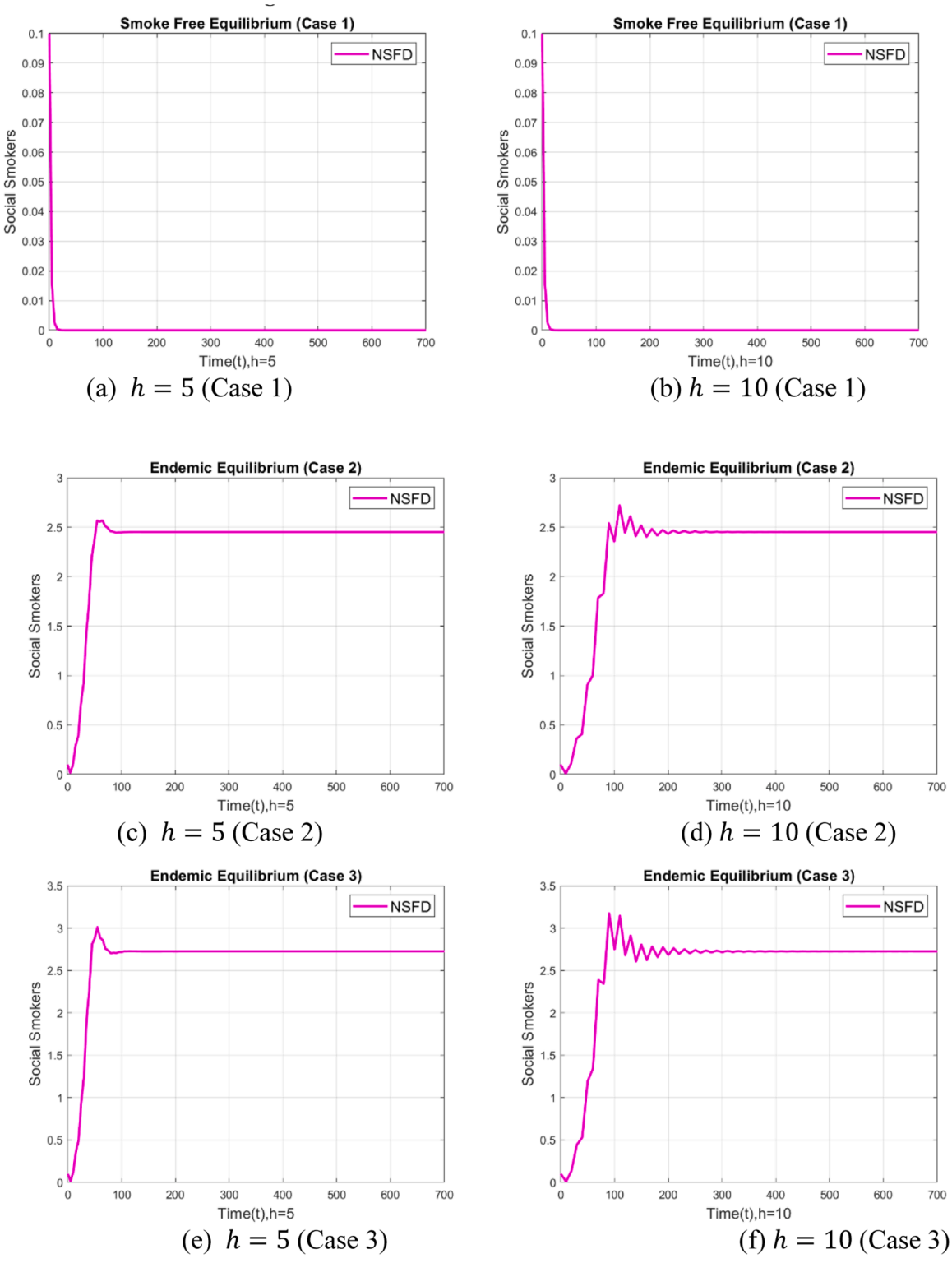


**Fig. 9.** Social smokers at various step sizes using the NSFD approach.

### 3.5. Boundedness of NSFD scheme

Given that the model is about the human population, it is critical to ensure that at any given time '$t$', the sum of populations in all compartments does not exceed the overall population. The following theorem addresses this condition effectively.

***Theorem:*** *Let* $P, S, R, Q,$ *and* $E \geq 0$ *are finite and* $P + S + R + Q + E \leq N$. *Furthermore,* $\geq 0$, $\varphi(\sigma) \geq 0$, $\psi(\sigma) \geq 0, \mu \geq 0, \omega_1 \geq 0, \omega_2 \geq 0, \geq 0, \tau_1 \geq 0, \tau_2 \geq 0$ *and* $\beta(\sigma) \geq 0$, *then they hold a constant such that* $P^{n+1} + S^{n+1} + R^{n+1} + Q^{n+1} + E^{n+1} \leq N_n$ *for all* $n \in Z^+$.

The proof is provided in Appendix A.2.

### 3.6. Convergence analysis

Convergence analysis ensures that the NSFD scheme approximates the continuous model accurately as the time step $h \to 0$. Using the Jaco-

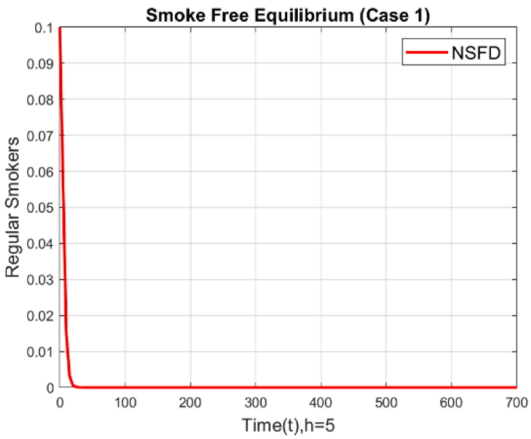


(a) $h = 5$ (Case 1)

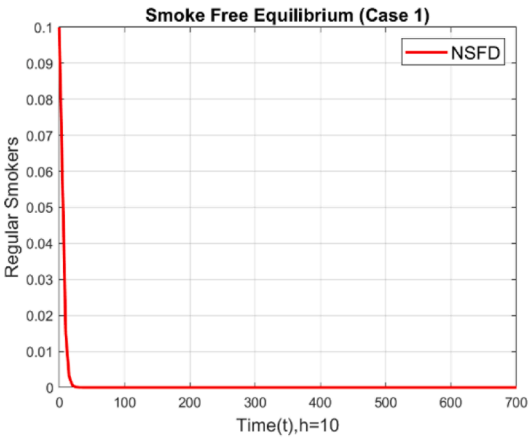


(b) $h = 10$ (Case 1)

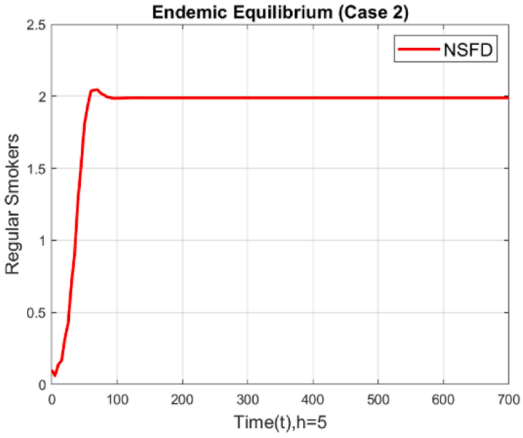


(c) $h = 5$ (Case 2)

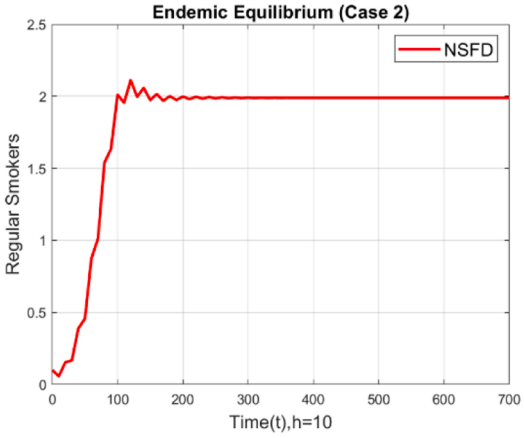


(d) $h = 10$ (Case 2)

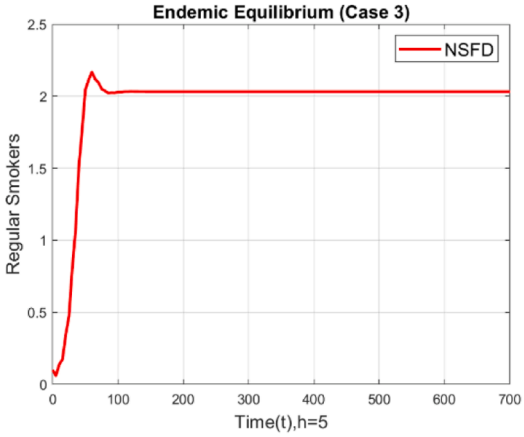


(e) $h = 5$ (Case 3)

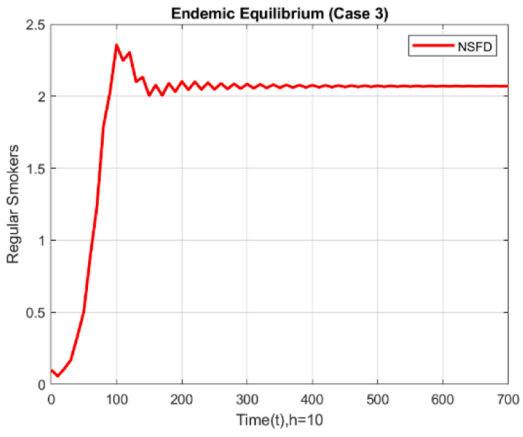


(f) $h = 10$ (Case 3)

**Fig. 10.** Regular smokers at various step sizes using the NSFD approach.

bian matrix at the SFE and eigenvalue analysis, it is shown that all eigenvalues lie strictly within the unit circle, ensuring convergence.

The detailed derivations and matrix computations are given in Appendix A.3.

### 3.7. Consistency analysis

Consistency means the closeness of the solutions of a numerical method to those of the continuous model as the higher computational parameters, like step size, are removed. The assessment also highlights the importance of maintaining stability in NSFD schemes in order to produce the most reliable numerical solutions possible. Values of the parameters used for simulation are shown in Table 1.

Beginning with the first equation in the system (16), we get

$$P^{n+1}(1+h(\beta(\sigma)R^n e^{-\mu\tau_1}+\mu)) = P^n \ + h\pi. \tag{17}$$

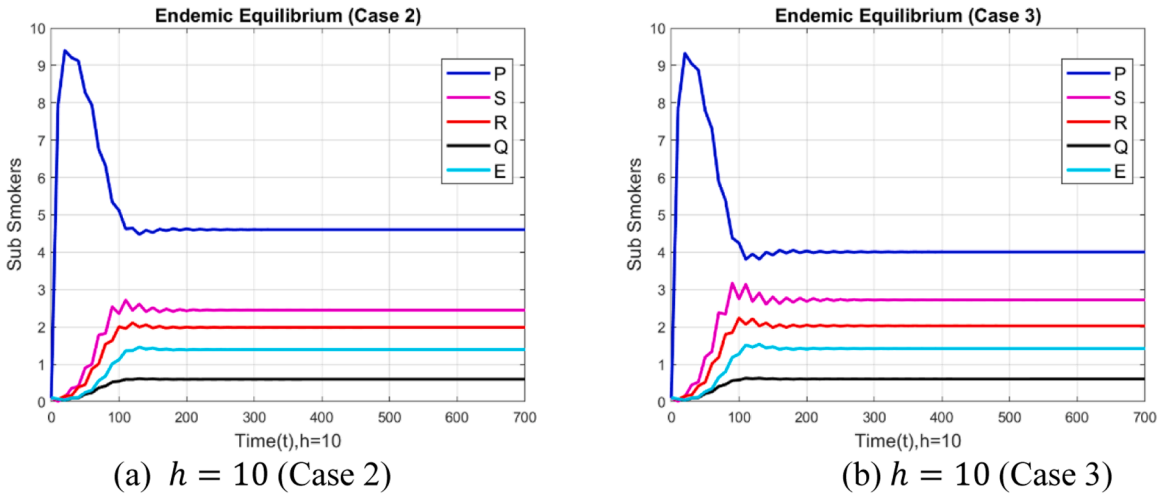


(a) $h = 10$ (Case 2) (b) $h = 10$ (Case 3)

**Fig. 11.** Compartmental comparison of the PSRQE smoking model using the NSFD approach.

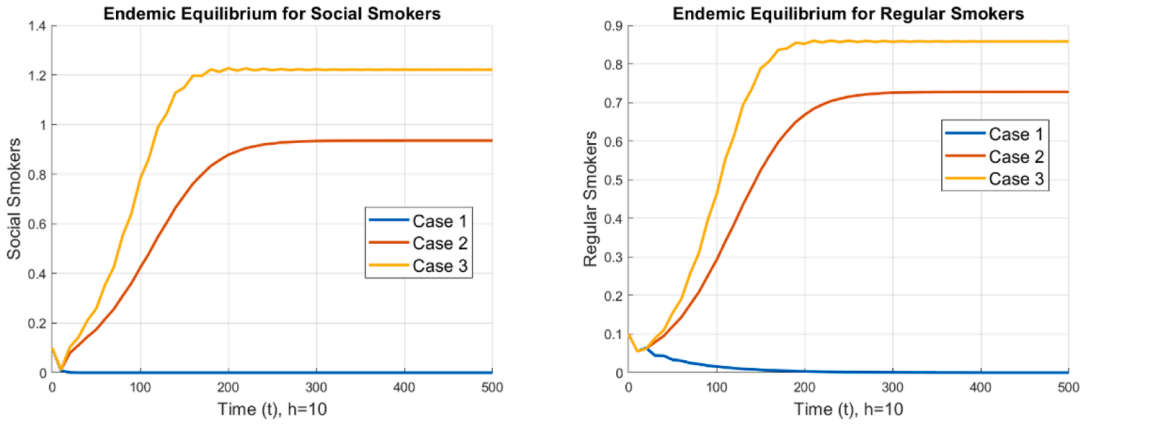


(a) $h = 10$ (Social Smokers) (b) $h = 10$ (Regular Smokers)

**Fig. 12.** Social and Regular smokers in each case, using the NSFD approach.

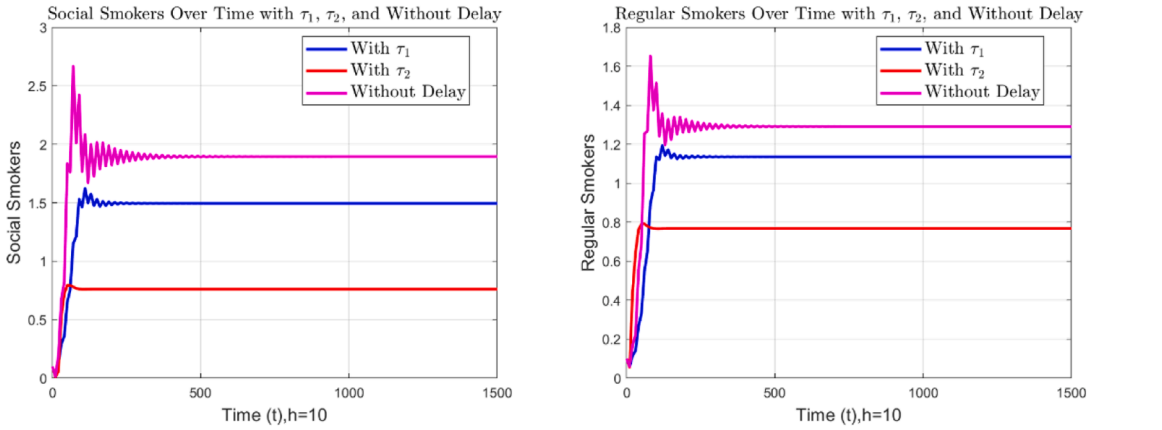


(a) $h = 10$ (Social Smokers) (b) $h = 10$ (Regular Smokers)

**Fig. 13.** Effect of Time Delay on Smokers using the NSFD approach.

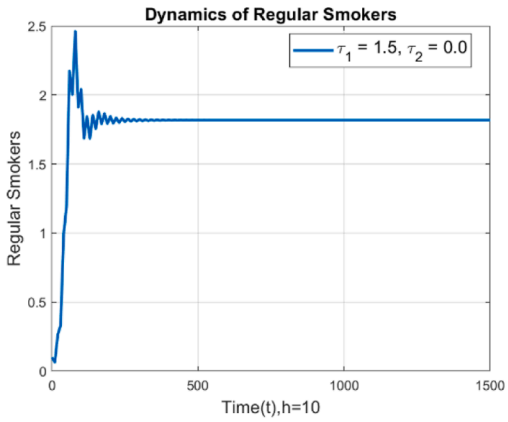


(a) $h = 10\ (\tau_1 = 1.5, \tau_2 = 0)$

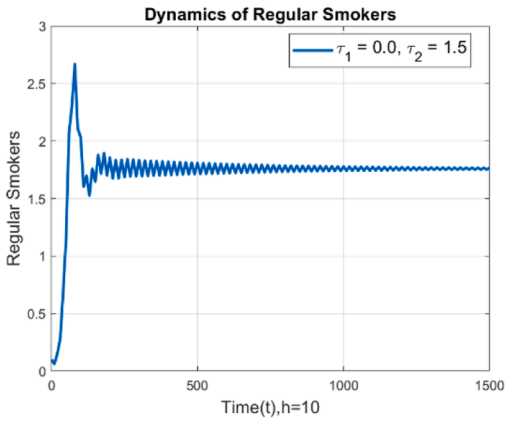


(b) $h = 10\ (\tau_1 = 0, \tau_2 = 1.5)$

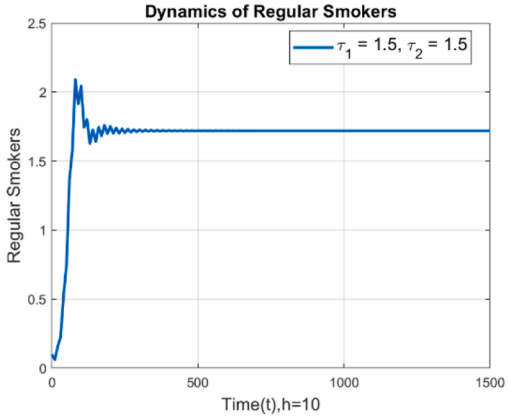


(c) $h = 10\ (\tau_1 = 1.5, \tau_2 = 1.5)$

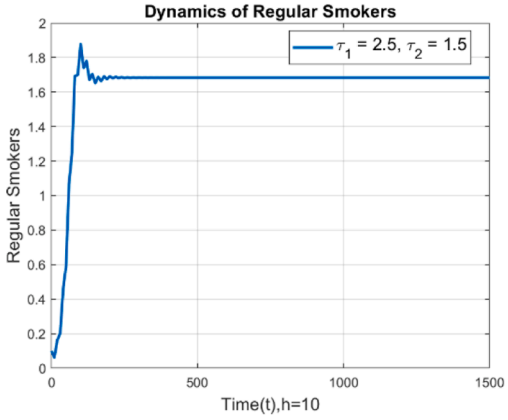


(d) $h = 10\ (\tau_1 = 2.5, \tau_2 = 1.5)$

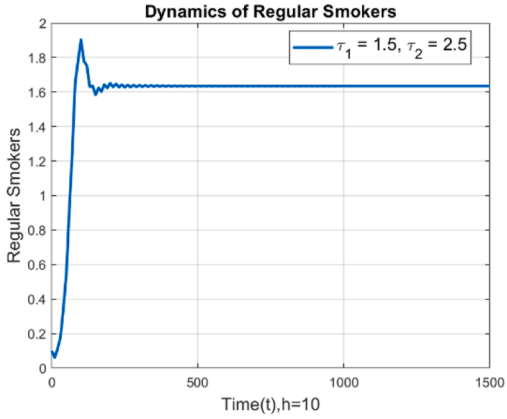


(e) $h = 10\ (\tau_1 = 1.5, \tau_2 = 2.5)$

**Fig. 14.** Dynamics of delays in Regular smokers.

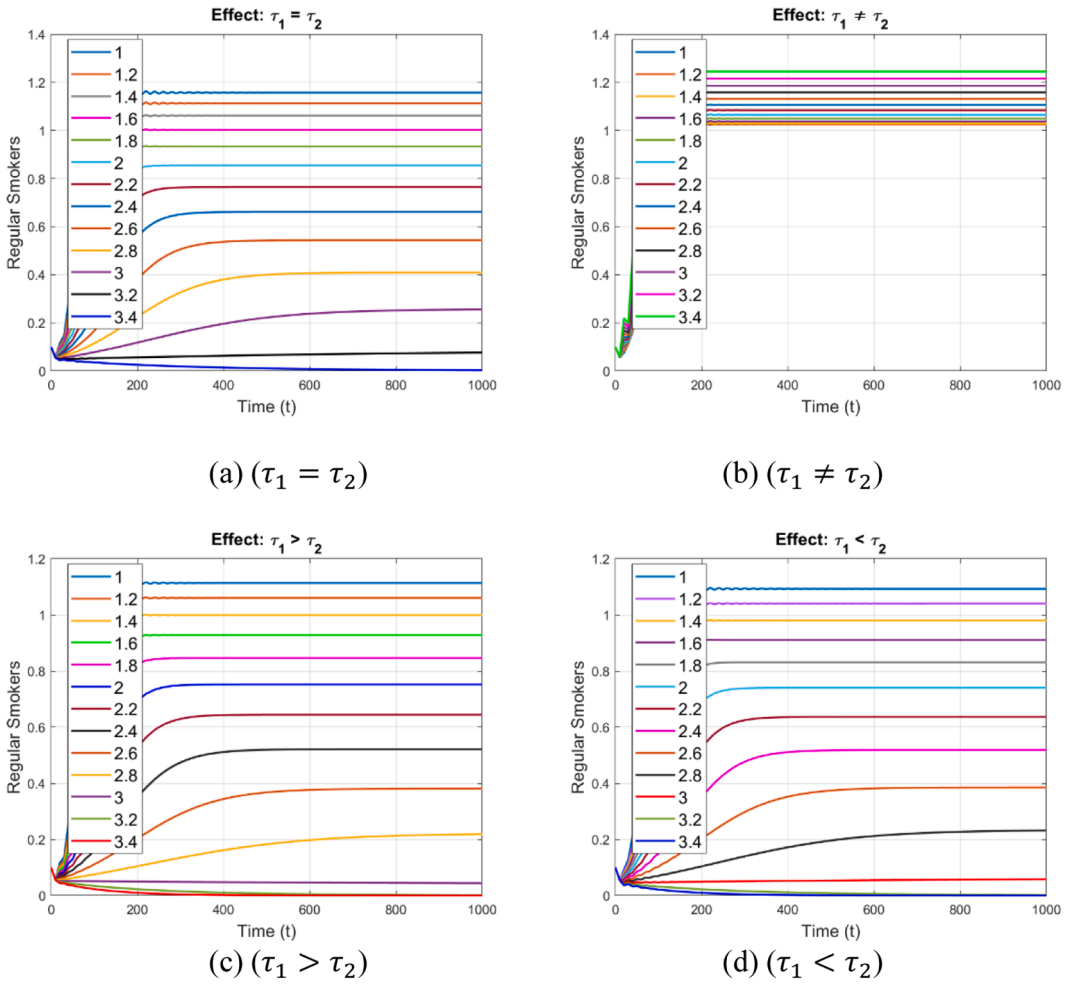


**Fig. 15.** Effect of time delay $\tau_1$ *and* $\tau_2$ on Social and Regular smokers.

**Table 2**
Comparison of the numerical schemes [56].

| $h$ | Euler | RK-4 | NSFD Scheme |
|---|---|---|---|
| **0.1** | Convergence (Positive) | Convergence (Positive) | Convergence (Positive) |
| **0.5** | Convergence (Positive) | Convergence (Positive) | Convergence (Positive) |
| **1** | Convergence (Positive) | Convergence (Positive) | Convergence (Positive) |
| **1.2** | Divergence (Negative) | Convergence (Positive) | Convergence (Positive) |
| **1.5** | Divergence (Negative) | Divergence (Negative) | Convergence (Positive) |
| **2** | Divergence (Negative) | Divergence (Negative) | Convergence (Positive) |
| **5** | Divergence (Negative) | Divergence (Negative) | Convergence (Positive) |
| **10** | Divergence (Negative) | Divergence (Negative) | Convergence (Positive) |
| **1000** | Divergence (Negative) | Divergence (Negative) | Convergence (Positive) |

The $P^{n+1}$ can be expressed using its Taylor series expansion as follows:

$$P^{n+1} = \left(P^n + h\frac{dP}{dt} + \frac{h^2}{2!}\frac{d^2P}{dt^2} + \frac{h^3}{3!}\frac{d^3P}{dt^3} + \ldots\right). \tag{18}$$

From Eq. (17), we obtain

$$\left(P^n + h\frac{dP}{dt} + \frac{h^2}{2!}\frac{d^2P}{dt^2} + \frac{h^3}{3!}\frac{d^3P}{dt^3} + \ldots\right)(1 + h(\beta(\sigma)R^n e^{-\mu\tau_1} + \mu)) = P^n + h\pi.$$

After simplifying and taking $h \to 0$, we obtain:

$$P^n(\beta(\sigma)R^n e^{-\mu\tau_1} + \mu) + \frac{dP}{dt} = \pi,$$

$$\frac{dS}{dt} = \pi - P^n\beta(\sigma)R^n e^{-\mu\tau_1} - \mu P^n,$$

$$\Rightarrow \frac{dS}{dt} = \pi - P\beta(\sigma)Re^{-\mu\tau_1} - \mu P.$$

From the second equation of the NSFD scheme (16), we have

$$S^{n+1}(1 + h(\omega_1 + \mu)) = S^n + h(\beta(\sigma)P^n R^n e^{-\mu\tau_1}). \tag{19}$$

The $S^{n+1}$ can be expressed using its Taylor series expansion as follows:

$$S^{n+1} = \left(S^n + h\frac{dS}{dt} + \frac{h^2}{2!}\frac{d^2S}{dt^2} + \frac{h^3}{3!}\frac{d^3S}{dt^3} + \ldots\right). \tag{20}$$

From Eq. (19), we obtain

$$\left(S^n + h\frac{dS}{dt} + \frac{h^2}{2!}\frac{d^2S}{dt^2} + \frac{h^3}{3!}\frac{d^3S}{dt^3} + \ldots\right)(1 + h(\omega_1 + \mu)) = S^n + h(\beta(\sigma)P^n R^n e^{-\mu\tau_1}).$$

After simplifying and taking $h \to 0$, we obtain:

$$S^n(\omega_1+\mu)+\frac{dS}{dt}= \beta(\sigma)P^nR^ne^{-\mu\tau_1},$$

$$\frac{dS}{dt}= \beta(\sigma)P^nR^ne^{-\mu\tau_1}-(\omega_1+\mu)S^n,$$

$$\frac{dS}{dt}= \beta(\sigma)PRe^{-\mu\tau_1}-(\omega_1+\mu)S.$$

From the third equation of the NSFD scheme (16), we have

$$R^{n+1}(1+h(\psi(\sigma)+\mu))=R^n+h(\omega_1S^n+\omega_2P^nQ^ne^{-\mu\tau_2}). \tag{21}$$

The $R^{n+1}$ can be expressed using its Taylor series expansion as follows:

$$R^{n+1}=\left(R^n+h\frac{dR}{dt}+\frac{h^2}{2!}\frac{d^2R}{dt^2}+\frac{h^3}{3!}\frac{d^3R}{dt^3}+\dots\right). \tag{22}$$

From Eq. (21), we obtain

$$\left(R^n+h\frac{dR}{dt}+\frac{h^2}{2!}\frac{d^2R}{dt^2}+\frac{h^3}{3!}\frac{d^3R}{dt^3}+\dots\right)(1+h(\psi(\sigma)+\mu))$$
$$=R^n+h(\omega_1S^n+\omega_2P^nQ^ne^{-\mu\tau_2}).$$

After simplifying and taking $h \to 0$, we obtain:

$$(\psi(\sigma)+\mu))R^n+\frac{dR}{dt}=\omega_1S^n+\omega_2P^nQ^ne^{-\mu\tau_2},$$

$$\frac{dR}{dt}= \omega_1S^n+\omega_2P^nQ^ne^{-\mu\tau_2}-(\psi(\sigma)+\mu))R^n,$$

$$\Rightarrow\frac{dR}{dt}=\omega_1S+\omega_2PQe^{-\mu\tau_2}-(\psi(\sigma)+\mu))R.$$

From the fourth equation of the NSFD scheme (16), we have

$$Q^{n+1}(1+h(\omega_2R^ne^{-\mu\tau_2}+\mu))=Q^n+h(\psi(\sigma)(1-\varphi(\sigma))R^n), \tag{23}$$

The $Q^{n+1}$ can be expressed using its Taylor series expansion as follows:

$$Q^{n+1}=\left(Q^n+h\frac{dQ}{dt}+\frac{h^2}{2!}\frac{d^2Q}{dt^2}+\frac{h^3}{3!}\frac{d^3Q}{dt^3}+\dots\right). \tag{24}$$

From Eq. (23), we obtain

$$\left(Q^n+h\frac{dQ}{dt}+\frac{h^2}{2!}\frac{d^2Q}{dt^2}+\frac{h^3}{3!}\frac{d^3Q}{dt^3}+\dots\right)(1+h(\omega_2R^ne^{-\mu\tau_2}+\mu))$$
$$=Q^n+h(\psi(\sigma)(1-\varphi(\sigma))R^n).$$

After simplifying and taking $h \to 0$ we obtain:

$$(\omega_2R^ne^{-\mu\tau_2}+\mu)Q^n+\frac{dQ}{dt}=\psi(\sigma)(1-\varphi(\sigma))R^n,$$

$$\frac{dQ}{dt}= \psi(\sigma)(1-\varphi(\sigma))R^n-(\omega_2R^ne^{-\mu\tau_2}+\mu)Q^n,$$

$$\Rightarrow\frac{dQ}{dt}= \psi(\sigma)(1-\varphi(\sigma))R-(\omega_2Re^{-\mu\tau_2}+\mu)Q.$$

From the Fifth equation of the NSFD scheme (16), we have

$$E^{n+1}(1+h\mu)=E^n+h\varphi(\sigma)\psi(\sigma)R^n, \tag{25}$$

The $E^{n+1}$ can be expressed using its Taylor series expansion as follows:

$$E^{n+1}=\left(E^n+h\frac{dE}{dt}+\frac{h^2}{2!}\frac{d^2E}{dt^2}+\frac{h^3}{3!}\frac{d^3E}{dt^3}+\dots\right). \tag{26}$$

From Eq. (25), we obtain

$$\left(E^n+h\frac{dE}{dt}+\frac{h^2}{2!}\frac{d^2E}{dt^2}+\frac{h^3}{3!}\frac{d^3E}{dt^3}+\dots\right)(1+h\mu)=E^n+h\varphi(\sigma)\psi(\sigma)R^n.$$

After simplifying and taking $h \to 0$, we obtain:

$$\mu E^n+\frac{dE}{dt}=\varphi(\sigma)\psi(\sigma)R^n,$$

$$\frac{dE}{dt}=\varphi(\sigma)\psi(\sigma)R^n-\mu E^n,$$

$$\Rightarrow\frac{dE}{dt}=\varphi(\sigma)\psi(\sigma)R-\mu E.$$

## 4. Mathematical simulations

### 4.1. Numerical simulation using forward Euler method

The forward Euler method illustrates the population dynamics across various step sizes, as shown in Fig. 3. The graph highlights the transitions between smoke-free and smoker-dominated stable states and non-physical oscillations in node values. Larger step sizes result in negative population values, which are unrealistic and unsuitable for modeling smoking behavior. This demonstrates that increasing the step size commonly leads to inaccurate and non-physical outcomes.

Fig. 4 focuses on the population of regular smokers under different step sizes, applying the forward Euler method. Similar to the transitions observed in other compartments, oscillations and adverse results occur, reaffirming the limitations of this method when larger step sizes are used.

In Fig. 5, the smoking model illustrates the dynamics of all compartments, emphasizing their interactions.

### 4.2. Numerical simulation using RK-4 method

Fig. 6 illustrates the population dynamics of social smokers under varying step sizes, using the RK-4 method.

Fig. 7 illustrates the population dynamics of regular smokers under varying step sizes, using the RK-4 method. Similar to the transitions observed in other compartments, oscillations, and unfavorable outcomes emerge, highlighting the limitations of this method when larger step sizes are applied.

In Fig. 8, the smoking model illustrates the dynamics of all compartments, emphasizing their interactions.

### 4.3. Numerical simulation using NSFD method

Fig. 9 showcases the dynamics of social smokers at various step sizes, demonstrating the effectiveness of this approach in eliminating negative values and improving model accuracy.

Fig. 10 confirms that the NSFD method maintains positive population values across all step sizes, particularly for the regular smoker compartment.

Fig. 11 confirms that the NSFD method maintains positive population values across all step sizes, particularly for the regular smoker compartment.

Fig. 12 evaluates the social and regular smoker population across different scenarios, highlighting variations in smoking prevalence. Case 1 shows a near-zero prevalence of smokers, while Cases 2 and 3 depict stable smoking rates, with Case 3 recording a higher smoking prevalence than Case 2.

Fig. 13 explores the impact of incorporating a delay factor into the fuzzy delayed NSFD model, showing that delays significantly reduce smoking prevalence.

The subfigures in Fig. 14 illustrate the impact of time-delay

parameters ($\tau_1$ and $\tau_2$) on the dynamics of regular smokers. In all cases, the steady-state value remains consistent, but transient behaviors vary significantly. When $\tau_1$ is present without $\tau_2$, the system stabilizes rapidly with minimal oscillations, while $\tau_2$ alone causes persistent oscillations and delays stabilization. A combination of $\tau_1$ and $\tau_2$ balances these effects, leading to moderate oscillations and intermediate stabilization times. In the last two graphs, different $\tau_1$ and $\tau_2$ values affect the speed of initial growth and the smoothness of oscillation damping, highlighting how these parameters shape transient dynamics without altering the equilibrium. The values of $\tau_1$ and $\tau_2$ in the last two graphs could be more significant for controlling smoking behavior. In these cases, the system stabilizes at a lower steady-state value.

It is seen in Fig. 15 that the dynamics of delaying individuals from becoming regular smokers are different under distinct time delays $\tau$ one and $\tau_2$. It is observed that while $\tau_1 = \tau_2$, the system demonstrated balanced behavior characterized by oscillatory processes and smooth convergence and, therefore, minimal interference with the potential delay of smoking. If $\tau_1 > \tau_2$, the larger $\tau_1$increases the duration of oscillatory behavior and retards stabilization, which makes this case especially useful in terms of the objective of slowing down the process of passing to regularly ritualized smoking. On the other hand, if $\tau_1 < \tau_2$, the small $\tau_1$ enhances the initial response while prolonging the convergence marginally, hence being ineffective. When there are no time delays $\tau_1 = \tau_2 = 0$, the system returns to a steady state without oscillation and with the shortest setting time, and this is considered to be a poor case. In particular, $\tau_1 > \tau_2$ is the most significant scenario for delaying the transition to regular smoking due to sustained oscillations and slower stabilization.

### 4.4. Comparative analysis of numerical schemes

The section then contrasts several numerical schemes relative to their potential to maintain convergence and positivity on different step sizes. One of the essential elements is numerical stability, especially when the models contain time delay and fuzzy parameters. So there is a demand to compare the efficiency of these schemes in preserving the qualitative dynamics of the system. Table 2 provides the convergence behavior of various schemes with numerical steps.

Table 2 illustrates that the NSFD scheme has higher levels of stability and maintains positivity, while ensuring convergence with a relatively high step size, *h*. Conversely, increasing the step size results in instability in the Euler and RK-4 procedures and, in most cases, leads to diverged or generates negative values, which goes against the fact that the NSFD procedure leads to a much more robust solution.

The present research provides practical implications for tobacco control policy and quitting planning. Numerical stability with the NSFD method is made possible by the capability of the algorithm to maintain positivity upon discretization of any step size (Fig. 11), which guarantees the possibility of reliable, scalable intervention forecasts. The very close to zero prevalence of Case 1 suggests early and intense intervention, such as school-based prevention. In contrast, stable but high prevalence of Cases 2 and 3 should maintain more extended cessation support, for instance, nicotine replacement or counseling in high-risk populations (Fig. 12). The prevalence decreases associated with delays (Fig. 13) highlight the advantage of timing cessation campaigns during natural behavioral transition lags (i.e., latency to initiation, $\tau_1$, quit attempts, $\tau_2$). The transient patterns formed by $\tau_1$one and $\tau_2$ (Fig. 14) also show that even in oscillatory conditions, additional support at vulnerable periods can have ameliorating effects on oscillatory effects, especially where only $\tau_1$contributes to delays. These results can inform an evidence-based approach to maximising smoking prevention and cessation and have implications given the health, social, and economic costs of tobacco smoking.

## 5. Conclusion

This research proposes a fuzzy PSRQE model to examine the transition between smoking perception and addresses the vagueness that may exist in real-life smoking patterns. Initiation probabilities, quitting success rates, relapse probabilities, and two-time delay variables, $\tau_1$ and $\tau_2$, are incorporated into the model to account for the stochasticity of smoking behavior. From these findings, it is clear that although the overall density of regular smokers is constant, the temporary patterns exhibit significant sensitivity to changes in $\tau_1$ and $\tau_2$. Of the two parameters, this reveals that introducing $\tau_1$ stabilizes the curve rather quickly, with only insignificant first-order oscillations, while $\tau_2$ results in sustained oscillations with slower stabilization. The sum of $\tau_1$ and $\tau_2$ is moderate, which results in final cases and smoker levels being somewhat lower, suggesting the potential for reducing smoking. The RK-4, forward Euler, and the NSFD numerical methods supplement the model's results to reveal its accuracy, while the latter maintains structural stability across large. It has also been seen that from the convergence analysis, the results are reliable, nonnegative, and bounded solutions. The delay variables are of significant interest in this study to demonstrate how transient dynamics affect smoking patterns. Using fuzzy theory and time delay variables, the present study developed a solid model of smoking behavior transitions that can help in identifying the dimensions leading to the appropriate changes in the behavior for the successful design of the required intervention. These results indicate the importance of specific strategies to decrease smoking rates and minimize health, social, and economic consequences, as the further applications of this model will be helpful for legislators and healthcare professionals.

## Future work

In the future, this study can be furthered by testing the theoretical model against real-world data. Whereas the mathematical basis of the model is established within the current exercise, it will be taken into account in our further work in order to maximize practical application of the model through resulting validation and calibration. Also, future work on this can be continued by bringing in 3D simulations via parametric grids (e.g., $\beta(\sigma)$ and $\tau_1$). This would provide a deeper understanding of the model dynamics, but this one can be undertaken in our future studies.

## Ethical statement - studies in humans and animals

This research did not involve any studies in humans or animals. Therefore, no ethical approval or consent was required or obtained for this manuscript.

## Ethics statement

Not applicable. This study does not involve human participants, animals, or data from social media.

Data Availability

All data generated or analyzed during this study are included in this published article. Additional materials may be available upon request from the corresponding author.

## Consent for publication

All authors have reviewed and approved the final manuscript and consent to its submission to the journal.

## CRediT authorship contribution statement

**Muhammad Tashfeen:** Writing – original draft, Software, Methodology, Conceptualization. **Hothefa Shaker Jassim:** Writing – original draft, Visualization, Methodology, Funding acquisition, Conceptualization. **Muhammad Aziz ur Rehman:** Writing – original draft, Validation, Methodology, Formal analysis, Conceptualization. **Fazal Dayan:** Writing – original draft, Supervision, Methodology, Investigation, Conceptualization. **Muhammad Adil Sadiq:** Writing – review & editing, Visualization, Software, Methodology, Data curation, Conceptualization. **Husam A. Neamah:** Writing – review & editing, Visualization, Supervision, Methodology, Funding acquisition, Formal analysis, Conceptualization.

## Declaration of competing interest

The authors declare that there are no conflicts of interest related to this work.

## Funding Statement

This research did not receive any specific grant from funding agencies in the public, commercial, or not-for-profit sectors.

## Appendices

### A.1 Proof of Positivity of NSFD

$$\begin{cases} P^{n+1} = \dfrac{P^n + h\pi}{1 + h(\beta(\sigma)R^n e^{-\mu\tau_1} + \mu)} \geq 0, \\ S^{n+1} = \dfrac{S^n + h\beta(\sigma)P^n R^n e^{-\mu\tau_1}}{1 + hk_1} \geq 0, \\ R^{n+1} = \dfrac{R^n + h(\omega_1 S^n + \omega_2 P^n Q^n e^{-\mu\tau_2})}{1 + hk_2} \geq 0, \\ Q^{n+1} = \dfrac{Q^n + h(\psi(\sigma)(1-\varphi(\sigma))R^n)}{1 + h(\omega_2 R^n e^{-\mu\tau_2} + \mu)} \geq 0, \\ E^{n+1} = \dfrac{E^n + h\varphi(\sigma)\psi(\sigma)R^n}{1 + h\mu} \geq 0. \end{cases} \tag{A1}$$

**Proof:** Now for $n = 0$ system (A1) becomes

$$\begin{cases} P^1 = \dfrac{P^0 + h\pi}{1 + h\left(\beta(\sigma)R^0 e^{-\mu\tau_1} + \mu\right)} \geq 0, \\ S^1 = \dfrac{S^0 + h\beta(\sigma)P^0 R^0 e^{-\mu\tau_1}}{1 + hk_1} \geq 0, \\ R^1 = \dfrac{R^0 + h\left(\omega_1 S^0 + \omega_2 P^0 Q^0 e^{-\mu\tau_2}\right)}{1 + hk_2} \geq 0, \\ Q^1 = \dfrac{Q^0 + h\left(\psi(\sigma)(1-\varphi(\sigma))R^0\right)}{1 + h\left(\omega_2 R^0 e^{-\mu\tau_2} + \mu\right)} \geq 0, \\ E^1 = \dfrac{E^0 + h\varphi(\sigma)\psi(\sigma)R^0}{1 + h\mu} \geq 0. \end{cases} \tag{A2}$$

Now for $n = 1$ system (A1) becomes

$$\begin{cases} P^2 = \dfrac{P^1 + h\pi}{1 + h\left(\beta(\sigma)R^1 e^{-\mu\tau_1} + \mu\right)} \geq 0, \\ S^2 = \dfrac{S^1 + h\beta(\sigma)P^1 R^1 e^{-\mu\tau_1}}{1 + hk_1} \geq 0, \\ R^2 = \dfrac{R^1 + h\left(\omega_1 S^1 + \omega_2 P^1 Q^1 e^{-\mu\tau_2}\right)}{1 + hk_2} \geq 0, \\ Q^2 = \dfrac{Q^1 + h\left(\psi(\sigma)(1-\varphi(\sigma))R^1\right)}{1 + h\left(\omega_2 R^1 e^{-\mu\tau_2} + \mu\right)} \geq 0, \\ E^2 = \dfrac{E^1 + h\varphi(\sigma)\psi(\sigma)R^1}{1 + h\mu} \geq 0. \end{cases} \tag{A3}$$

Consider the above set of equations ensures the positive values of $P,\ S,\ R,\ Q$, and $E$ for $n = 2,\ 3,\ 4,\ldots,n-1$. In other words, for $n = 2,\ 3,\ 4,\ldots,\ n-1$, $P^{n+1} \geq 0,\ S^{n+1} \geq 0, R^{n+1} \geq 0, Q^{n+1} \geq 0$, and $E^{n+1} \geq 0$. Specifically, positivity will now be discussed for an arbitrary positive integer $n$, and it becomes clear that,

$$\begin{cases} P^{n+1} = \dfrac{P^n + h\pi}{1 + h(\beta(\sigma)R^n e^{-\mu\tau_1} + \mu)} \geq 0, \\ S^{n+1} = \dfrac{S^n + h\beta(\sigma)P^n R^n e^{-\mu\tau_1}}{1 + hk_1} \geq 0, \\ R^{n+1} = \dfrac{R^n + h(\omega_1 S^n + \omega_2 P^n Q^n e^{-\mu\tau_2})}{1 + hk_2} \geq 0, \\ Q^{n+1} = \dfrac{Q^n + h(\psi(\sigma)(1-\varphi(\sigma))R^n)}{1 + h(\omega_2 R^n e^{-\mu\tau_2} + \mu)} \geq 0, \\ E^{n+1} = \dfrac{E^n + h\varphi(\sigma)\psi(\sigma)R^n}{1 + h\mu} \geq 0. \end{cases} \tag{A4}$$

Obviously, $P^{n+1} \geq 0$, $S^{n+1} \geq 0$, $R^{n+1} \geq 0$, $Q^{n+1} \geq 0$, and $E^{n+1} \geq 0$ for all $n \in Z^+$.

**A.2 Proof of Boundedness of NSFD**

To ensure the boundedness of the NSFD scheme, from Eq. (16), we have:

$$\begin{aligned} &P^{n+1}(1 + h(\beta(\sigma)R^n e^{-\mu\tau_1} + \mu)) + S^{n+1}(1 + h(\omega_1 + \mu)) + R^{n+1}(1 + h(\psi(\sigma) + \mu)) + Q^{n+1}(1 + h(\omega_2 R^n e^{-\mu\tau_2} + \mu)) + E^{n+1}(1 + h\mu) \\ &= P^n + h\pi + S^n + h(\beta(\sigma)P^n R^n e^{-\mu\tau_1}) + R^n + h(\omega_1 S^n + \omega_2 P^n Q^n e^{-\mu\tau_2}) + Q^n + h(\psi(\sigma)(1-\varphi(\sigma))R^n) + E^n + h\varphi(\sigma)\psi(\sigma)R^n \end{aligned} \tag{A5}$$

$$\begin{aligned} &\left(P^{n+1} + S^{n+1} + R^{n+1} + Q^{n+1} + E^{n+1}\right)(1 + h\mu) + h(\beta(\sigma)R^n e^{-\mu\tau_1} + \omega_1 + \psi(\sigma) + \omega_2 R^n e^{-\mu\tau_2}) \\ &= (P^n + S^n + R^n + Q^n + E^n) + h(\pi + \beta(\sigma)P^n R^n e^{-\mu\tau_1} + \omega_1 S^n + \omega_2 P^n Q^n e^{-\mu\tau_2} + \psi(\sigma)(1-\varphi(\sigma))R^n + \varphi(\sigma)\psi(\sigma)R^n), \end{aligned} \tag{A6}$$

$$\left(P^{n+1} + S^{n+1} + R^{n+1} + Q^{n+1} + E^{n+1}\right) + G = \frac{(P^n + S^n + R^n + Q^n + E^n) + h(\pi + \beta(\sigma)P^n R^n e^{-\mu\tau_1} + \omega_1 S^n + \omega_2 P^n Q^n e^{-\mu\tau_2} + \psi(\sigma)(1-\varphi(\sigma))R^n + \varphi(\sigma)\psi(\sigma)R^n),}{(1 + h\mu)}. \tag{A7}$$

Where $G = h(\beta(\sigma)R^n e^{-\mu\tau_1} + \omega_1 + \psi(\sigma) + \omega_2 R^n e^{-\mu\tau_2})$

Now, for $n = 0$ system (A7) becomes

$$\left(P^1 + S^1 + R^1 + Q^1 + E^1\right) + G = \frac{\left(P^0 + S^0 + R^0 + Q^0 + E^0\right) + h\left(\pi + \beta(\sigma)P^0 R^0 e^{-\mu\tau_1} + \omega_1 S^0 + \omega_2 P^0 Q^0 e^{-\mu\tau_2} + \psi(\sigma)(1-\varphi(\sigma))R^0 + \varphi(\sigma)\psi(\sigma)R^0\right),}{(1 + h\mu)}.$$

Since $N_1 = P^0 + S^0 + R^0 + Q^0 + E^0$,

$P^1 + S^1 + R^1 + Q^1 + E^1, \leq N_1$.

Similarly, for $n \epsilon Z^+$system (A7) becomes

$$\left(P^{n+1} + S^{n+1} + R^{n+1} + Q^{n+1} + E^{n+1}\right) + G = \frac{(P^n + S^n + R^n + Q^n + E^n) + h(\pi + \beta(\sigma)P^n R^n e^{-\mu\tau_1} + \omega_1 S^n + \omega_2 P^n Q^n e^{-\mu\tau_2} + \psi(\sigma)(1-\varphi(\sigma))R^n + \varphi(\sigma)\psi(\sigma)R^n),}{(1 + h\mu)}. \tag{A8}$$

Consequently, $P^{n+1} + S^{n+1} + R^{n+1} + Q^{n+1} + E^{n+1} \leq N_n$ for all $n \in Z^+$, hence the proof.

**A.3 Proof of Convergence of NSFD**

$$\begin{cases} C_1 = \dfrac{P + h\pi}{1 + h(\beta(\sigma)Re^{-\mu\tau_1} + \mu)}, \\ C_2 = \dfrac{S + h\beta(\sigma)PRe^{-\mu\tau_1}}{1 + hk_1}, \\ C_3 = \dfrac{R + h(\omega_1 S + \omega_2 PQe^{-\mu\tau_2})}{1 + hk_2}, \\ C_4 = \dfrac{Q + h(\psi(\sigma)(1-\varphi(\sigma))R)}{1 + h(\omega_2 Re^{-\mu\tau_2} + \mu)}, \\ C_5 = \dfrac{E + h\varphi(\sigma)\psi(\sigma)R}{1 + h\mu}. \end{cases} \tag{A9}$$

The Jacobian matrix at the SFE is expressed as follows:

$$\mathscr{J}\left(\mathrm{E}_{\mathrm{p}}^0\right) = \begin{bmatrix} \dfrac{1}{1+h\mu} & 0 & 0 & 0 & 0 \\ 0 & \dfrac{1}{1+hk_1} & 0 & 0 & 0 \\ 0 & \dfrac{h\omega_1}{1+hk_2} & \dfrac{1}{1+hk_2} & 0 & 0 \\ 0 & 0 & 0 & \dfrac{1}{1+h\mu} & 0 \\ 0 & 0 & 0 & 0 & \dfrac{1}{1+h\mu} \end{bmatrix}$$

Eigenvalues of the above Jacobian matrix $\lambda_1 = 0.8 < 1, \lambda_2 = 0.625 < 1, \lambda_3 = 0.6452 < 1, \lambda_4 = 0.8 < 1,$ and $\lambda_5 = 0.8 < 1$. All the eigenvalues of the Jacobian matrix will lie within the unit circle, thereby ensuring the convergence of the proposed NSFD scheme at the SFE point at $E_p^0$.

## References


[1] World Health Organization. Tobacco fact. Available from: https://www.who.int/news-room/fact-sheets/detail/tobacco. 2023.
[2] N.L. Benowitz, Nicotine addiction, N. Engl. J. Med 362 (24) (2010) 2295–2303.
[3] Centers for Disease Control and Prevention. Smoking & tobacco use: health effects. Available from: https://www.cdc.gov/tobacco. 2020.
[4] M. Alomar, et al., Pesticides in tobacco smoke and lung cancer risk, Environ Health Perspect 129 (6) (2021) 067008.
[5] D.J. Handelsman, A.J. Conway, L.M. Boylan, J.R. Turtle, Testicular function in potential sperm donors: normal ranges and the effects of smoking and varicocele, Int J. Androl. 7 (5) (1984) 369–382.
[6] World Health Organization, MPOWER: a Policy Package to Reverse the Tobacco Epidemic, WHO, Geneva, 2008.
[7] R. West, et al., Smoking cessation interventions: a review, Lancet 385 (9987) (2015) 949–959.
[8] A. Din, et al., A fractional-order differential equation model of the smoking epidemic with relapse and harmonic mean type incidence rate, Fract Fract 7 (5) (2023) 370.
[9] M. Abdullah, A. Ahmad, N. Raza, M. Farman, M. Ahmad, Approximate solution and analysis of smoking epidemic model with Caputo fractional derivatives, Int. J. Appl. Comput. Math 4 (5) (2018) 112.
[10] Q. Haidong, M.U. Rahman, M. Arfan, Fractional model of smoking with relapse and harmonic mean type incidence rate under Caputo operator, J. Appl. Math Comput 69 (1) (2023) 403–420.
[11] S. Ullah, et al., Optimal control analysis of a smoking model with an education campaign, Chaos 28 (10) (2018) 103101.
[12] Y.N. Anjam, et al., A fractional order investigation of the smoking model using Caputo-Fabrizio differential operator, Fract. Fract 6 (11) (2022) 623.
[13] A.M.S. Mahdy, M.S. Mohamed, K.A. Gepreel, A. Al-Amiri, M. Higazy, Dynamical characteristics and signal flow graph of a nonlinear fractional smoking mathematical model, Chaos, Solit., Fractals 141 (2020) 110308.
[14] E. Addai, L. Zhang, J.K. Asamoah, J.F. Essel, A fractional order age-specific smoke epidemic model, Appl. Math Model 119 (2023) 99–118.
[15] E. Addai, A. Adeniji, O.J. Peter, J.O. Agbaje, K. Oshinubi, Dynamics of age-structure smoking models with government intervention coverage under fractal-fractional order derivatives, Fract Fract 7 (5) (2023) 370.
[16] M.A. Khan, et al., Analysis of a fractional smoking epidemic model with smoking relapse, Appl. Math Model 120 (2023) 168–187.
[17] R. Ross, The Prevention of Malaria, John Murray, London, 1911.
[18] W.O. Kermack, A.G. McKendrick, Contributions to the mathematical theory of epidemics—I, Bull Math Biol 53 (1–2) (1991) 33–55.
[19] P. Van den Driessche, J. Watmough, Reproduction numbers and sub-threshold endemic equilibria for compartmental models of disease transmission, Math Biosci 180 (1–2) (2002) 29–48.
[20] En'Ko P.D. In the course of epidemics of some infectious diseases. 1989.
[21] F. Brauer, C. Castillo-Chavez, Z. Feng, Mathematical Models in Epidemiology, Springer, New York, 2019.
[22] B. Buonomo, N. Chitnis, A. d'Onofrio, Seasonality in epidemic models: a literature review, Ric. Mat 67 (2018) 7–25.
[23] B. Buonomo, D. Lacitignola, C. Vargas-De-León, Qualitative analysis and optimal control of an epidemic model with vaccination and treatment, Math Comput. Simul 100 (2014) 88–102.
[24] H.W. Hethcote, The mathematics of infectious diseases, SIAM Rev 42 (4) (2000) 599–653.
[25] D.L. Martin, T.L. Gustafson, J.W. Pelosi, L. Suarez, G.V. Pierce, Contaminated produce—A common source for two outbreaks of Shigella gastroenteritis, Am J Epidemiol 124 (2) (1986) 299–305.
[26] W. Swaddiwudhipong, S. Karintraratana, S. Kavinum, A common-source outbreak of shigellosis involving a piped public water supply in northern Thai communities, J. Trop Med Hyg 98 (1995) 145.
[27] S. Momani, I.M. Batiha, I. Bendib, A. Al-Nana, A. Ouannas, M. Dalah, On finite-time stability of some COVID-19 models using fractional discrete calculus, Comput. Meth. Prog. Biomed. Update 7 (2025) 100188.
[28] J.Z. Ndendya, J.A. Mwasunda, S. Edward, N.S Mbare, A Caputo fractional-order model with MCMC for rabies transmission dynamics, Comput. Meth. Prog. Biomed. Update 7 (2025) 100206.
[29] E. Renald, M. Amadi, H. Haario, J. Buza, J.M. Tchuenche, V.G. Masanja, A comparative approach to analyzing data uncertainty in parameter estimation for a lumpy skin disease model, Comput. Meth. Prog. Biomed. Update 7 (2025) 100178.
[30] S.W. Teklu, B.S. Kotola, Insight into the treatment strategy on pneumonia transmission with asymptomatic carrier stage using a fractional order modeling approach, Comput. Meth. Prog. Biomed. Update 5 (2024) 100134.
[31] A.K. Misra, A. Sharma, J.B. Shukla, Modeling and analysis of the effects of awareness programs by the media on the spread of infectious diseases, Math Comput. Model 53 (5–6) (2011) 1221–1228.
[32] F.A. Rihan, Delay Differential Equations and Applications to Biology, Springer, Singapore, 2021, pp. 123–141.
[33] K.L. Cooke, J.A. Yorke, Some equations model growth processes and gonorrhea epidemics, Math Biosci 16 (1–2) (1973) 75–101.
[34] H.L. Smith, An Introduction to Delay Differential Equations With Applications to the Life Sciences, Springer, New York, 2011, pp. 119–130.
[35] editorsF. Brauer, C. Castillo-Chavez (Eds.), Mathematical Models For Communicable Diseases, SIAM, Philadelphia, 2012.
[36] S. Ghosh, V. Volpert, M. Banerjee, An epidemic model with time delay determined by the disease duration, Mathematics 10 (15) (2022) 2561.
[37] M. Meziane, A. Moussaoui, V. Volpert, On a two-strain epidemic model involving delay equations, Math Biosci. Eng 20 (12) (2023) 20683–20711.
[38] B.M. Almuqati, F.M. Allehiany, Global stability of a multi-group delayed epidemic model with logistic growth, AIMS Math 8 (10) (2023) 23046–23061.
[39] E. Fadhal, A. Raza, E.M. Rocha, W.F. Alfwzan, M. Rafiq, N. Ahmed, M. Bilal, Dynamical analysis of scabies delayed epidemic model with second-order global stability, PLoS One 20 (4) (2025) e0319095.
[40] A. Raza, U. Shafique, M.M. Al-Shamiri, N.M. Brites, Fadhal E. Computational analysis of hepatitis B epidemic model with incorporating a delay effect into stochastic differential equations, Math Meth. Appl. Sci 48 (10) (2025) 10361–10375.
[41] F. Minhós, A. Raza, U. Shafique, An efficient computational analysis for stochastic fractional heroin model with artificial decay term, AIMS Math 10 (3) (2025).
[42] R.M. Hussien, R.K. Naji, The dynamics of a delayed eco-epidemiological model with a nonlinear incidence rate, J. Appl. Math (2023).
[43] W. Shatanawi, A. Raza, M.S. Arif, M. Rafiq, K. Abodayeh, M. Bibi, An effective numerical method for the solution of a stochastic coronavirus (2019-nCoV) pandemic model, Comput. Mater Continua 66 (2) (2021) 1121–1137.
[44] M. Abdy, S. Side, S. Annas, W. Nur, W. Sanusi, An SIR epidemic model for COVID-19 spread with fuzzy parameter: the case of Indonesia, Adv. Differ. Equ. 2021 (2021) 1–7.
[45] C. Li, J. Huang, Y.H. Chen, H. Zhao, A fuzzy susceptible-exposed-infected-recovered model based on the confidence index, Int. J. Fuzzy Syst 23 (2021) 907–917.
[46] X. Shi, J. Li, A. Huang, S. Song, Z. Yang, Assessing the outbreak risk of epidemics using fuzzy evidential reasoning, Risk Anal 41 (11) (2021) 2046–2064.
[47] E.W. Stiegelmeier, G.M. Bressan, A fuzzy approach in the study of the COVID-19 pandemic in Brazil, Res Biomed Eng 37 (2021) 263–271.
[48] W.M. Shaban, A.H. Rabie, A.I. Saleh, Abo-Elsoud MA, Detecting COVID-19 patients based on a fuzzy inference engine and a deep neural network, Appl. Soft. Comput 99 (2021) 106906.
[49] G. Bhuju, G.R. Phaijoo, D.B. Gurung, Fuzzy approach analyzing SEIR-SEI dengue dynamics, Biomed Res. Int 2020 (2020) 1508613.
[50] M.M. Alqarni, M. Rafiq, F. Dayan, J. Awrejcewicz, N. Ahmed, A. Raza, M. O. Ahmad, W. Pawłowski, E.E Mahmoud, New trends in fuzzy modeling through numerical techniques, Comput. Mater Continua. 74 (3) (2023) 6371–6388.
[51] M.S. Arif, K. Abodayeh, Y. Nawaz, A hybrid SIR-fuzzy model for epidemic dynamics: a numerical study, CMES Comput. Model Eng. Sci 139 (3) (2024).
[52] L.C. De Barros, R.C. Bassanezi, W.A. Lodwick, First Course in Fuzzy logic, Fuzzy Dynamical systems, and Biomathematics, Springer, Berlin, 2016.
[53] Y.T. Mangongo, J.D.K. Bukweli, J.D.B. Kampempe, Fuzzy global stability analysis of the dynamics of malaria with fuzzy transmission and recovery rates, Am. J. Oper Res 11 (6) (2021) 257–282.
[54] K. Pavani, K. Raghavendra, A novel technique to study the solutions of the time-fractional nonlinear smoking epidemic model, Sci. Rep 14 (1) (2024) 4159.
[55] N. Chitnis, J.M. Hyman, J.M. Cushing, Determining important parameters in the spread of malaria through the sensitivity analysis of a mathematical model, Bull Math Biol 70 (2008) 1272–1295.
[56] M. Rafiq, N. Ahmed, M. Rafique, Ahmad MO, A reliable numerical analysis of transmission dynamics of chicken pox (varicella zoster virus), Sci. Inq. Rev 4 (4) (2020) 31–45.